

Application of Signomial Programming to Aircraft Design

Philippe G. Kirschen*, Martin A. York[†], Berk Ozturk[‡], and Warren W. Hoburg[§]

Massachusetts Institute of Technology, Cambridge, MA 02139

Due to the coupled nature of aircraft design, it is important to consider all major subsystems when optimizing a configuration. This is difficult when each individual subsystem model can be arbitrarily complex. By restricting an optimization problem to have a certain mathematical structure, significantly more effective and tractable solution techniques can be used. Geometric programming, one such technique, guarantees finding a globally optimal solution. Although it has been shown that geometric programming can be used to solve some aircraft design problems, the required formulation can prove too restrictive for certain relationships. Signomial programming is a relaxation of geometric programming that offers enhanced expressiveness. Although they do not guarantee global optimality, solution methods for signomial programs are disciplined and effective. In this work, signomial programming models are proposed for optimal sizing of the tail, fuselage, landing gear, and wing of a commercial aircraft. These models are combined together to produce a full aircraft optimization model. Signomial programming's formulation allows it to handle some key constraints in aircraft design, and therefore an improvement in fidelity over geometric programming models is achieved. A primary contribution of this work is to demonstrate signomial programming as a viable tool for multidisciplinary aircraft design optimization.

I. Introduction

Geometric Programming (GP)^a is an optimization technique that combines the expressiveness of non-linear objectives and constraints with the mathematical rigor of convex optimization to provide a powerful approach to solving multidisciplinary aircraft design optimization problems. For problems that can be formulated as Geometric Programs (GPs), modern solvers guarantee *globally* optimal solutions, are extremely fast, and return local sensitivities at no extra cost, thanks to the principle of Lagrange duality. In previous work, Hoburg [1] shows that many models common to aircraft design can be represented directly in GP-compatible form, and that there are a number

*Graduate student, Department of Aeronautics and Astronautics; currently Optimization Engineer, Hyperloop One. AIAA Student Member.

[†]Graduate Student, Department of Aeronautics and Astronautics; currently Second Lieutenant, United States Air Force.

[‡]Graduate student, Department of Aeronautics and Astronautics. AIAA Student Member.

[§]Assistant Professor, Department of Aeronautics and Astronautics; currently Astronaut Candidate, NASA. AIAA Member.

^aThe “GP” acronym is overloaded, referring both to geometric programs - the class of optimization problem discussed in this work - and geometric programming - the practice of using such programs to model and solve optimization problems. The same is true of the “SP” acronym.

of innovative ways of dealing with models that cannot, including, but not limited to, changes of variables and GP-compatible fitting methods. Finally, it is also shown that such problems can be solved efficiently using a standard laptop computer. The aircraft design problem solved in [1] includes models for steady level flight, range, takeoff, landing, a sprint flight condition, actuator disk propulsive efficiency, simple drag and weight buildups, and a beam wing box structure.

Due to these promising initial results, there is a strong desire to extend the use of GP for aircraft design both in breadth, by considering more aspects of the aircraft design problem, and in depth, by increasing the fidelity of the models used. Unfortunately, the restrictions of the GPs formulation mean that not all aircraft design constraints can be readily implemented as part of a GP. A generalization of GP called Signomial Programming (SP) helps to address this by allowing constraints with less restrictive formulations [2]. A relatively small relaxation in the restriction on problem formulation means that SP can handle a significantly more general set of problems than GP, but this comes at a cost: SP does not boast the same guarantee of global optimality as GP. Despite this, solution methods remain disciplined and effective by leveraging a *difference of convex program* formulation for SP.

Signomial programming is important for aircraft design because it allows a modeller to leverage the speed and reliability of GP on models that are not GP-compatible, and it enables increasing fidelity where it is not possible to maintain GP-compatibility. From the authors' limited experience, only a small proportion of the constraints in aircraft design models require signomials, if any. In many cases, however, omitting these constraints would mean failing to capture an important design consideration. Sometimes, the constraint in question is the only constraint that keeps one or more design variables meaningfully bounded. Thus, optimization quality and robustness are sacrificed in exchange for obtaining dual feasibility and/or higher model fidelity. It is important to stress that the purpose of this work is not to use SP liberally, but rather to use it in a targeted and precise manner, where the marginal cost of introducing a signomial constraint can be justified by an adequate increase in model fidelity or accuracy. Because they result in convex restrictions on the feasible set, monomial and posynomial constraints are still viewed as the preferred approach wherever possible.

There exists extensive research in Multidisciplinary Design Optimization (MDO) methods for conceptual aircraft design [3–7]. Of the many different frameworks in the literature, TASOPT [5] is particularly relevant to the present work because of its use of physics based models, medium fidelity analytical models, and multidisciplinary considerations of aircraft subsystems. Common challenges faced in multidisciplinary design optimization include models that are too computationally expensive to be practical for a designer; final results that are sensitive to the choice of baseline design; evaluations of black box functions that offer optimizers little-to-no visibility of exploitable mathematical structure; and coupling of different analysis tools that require delicate wiring between models, and generally another layer of complexity and opacity.

In the following sections, SP models are presented for design of the wing, vertical tail, horizontal tail, fuselage and landing gear of a conventional tube-and-wing commercial aircraft. These models can be used to determine optimal values for, among other things, the preliminary geometry, positioning and weight of each subsystem. They are a compilation of constraints, some developed by the authors and others obtained from a variety of references. As a result, the relationships are not necessary original, but their adaptation to signomial programming is. Each model is readily extensible, meaning constraints can be added and made more sophisticated with ease.

Each section of this paper describes a model, beginning with the key assumptions regarding the model, followed by the enumeration and description of the constraints. The intention is to demon-

strate the wide range of aircraft design constraints that fit naturally into the signomial programming formulation.

The models are combined together in a full-configuration system-level model that captures the highly coupled nature of aircraft design. This model is solved using estimates for fixed variables based on a reference aircraft, the Boeing 737-800. Although the emphasis of this work is not on the solution, it does allow us to verify that the full-system model has a solution that is not only feasible, but also credible. To the authors' best knowledge, this is the first published work on SP applied to aircraft design.

Before presenting these models, we begin with brief introductions to both geometric and signomial programming.

A. Introduction to Geometric Programming

First introduced in 1967 by Duffin, Peterson, and Zener [8], a GP is a specific type of constrained, nonlinear optimization problem that becomes convex after a logarithmic change of variables. Modern GP solvers employ primal-dual interior point methods [9] and are extremely fast. A typical sparse GP with tens of thousands of decision variables and one million constraints can be solved on a desktop computer in minutes [2]. Furthermore, these solvers do not require an initial guess and guarantee convergence to a *global* optimum, whenever a feasible solution exists. Being able to find optimal solutions without an initial guess makes the technique particularly useful for conceptual aircraft design, where it is important that results are not biased by preconceptions of how an optimal aircraft should look.

These impressive properties are possible because GPs represent a restricted subset of nonlinear optimization problems. In particular, the objective and constraints can only be composed of *monomial* and *posynomial* functions.

A *monomial* is a function of the form

$$m(\mathbf{x}) = c \prod_{j=1}^n x_j^{a_j}, \quad (1)$$

where $a_j \in \mathbb{R}$, $c \in \mathbb{R}_{++}$, and $x_j \in \mathbb{R}_{++}$. For instance, the familiar expression for lift, $\frac{1}{2}\rho V^2 C_L S$, is a monomial with $\mathbf{x} = (\rho, V, C_L, S)$, $c = 1/2$, and $\mathbf{a} = (1, 2, 1, 1)$.

A *posynomial* is a function of the form

$$p(\mathbf{x}) = \sum_{k=1}^K c_k \prod_{j=1}^n x_j^{a_{jk}}, \quad (2)$$

where $\mathbf{a}_k \in \mathbb{R}^n$, $c_k \in \mathbb{R}_{++}$, and $x_j \in \mathbb{R}_{++}$. Thus, a posynomial is simply a sum of monomial terms, and all monomials are also posynomials (with just one term).

In plain English, a GP minimizes a posynomial objective function, subject to monomial equality constraints and posynomial inequality constraints. The standard form of a geometric program in mathematical notation is as follows:

$$\begin{aligned} & \text{minimize } p_0(\mathbf{x}) \\ & \text{subject to } p_j(\mathbf{x}) \leq 1, \quad j = 1, \dots, n_p, \\ & \quad m_k(\mathbf{x}) = 1, \quad k = 1, \dots, n_m, \end{aligned} \quad (3)$$

where the p_i are posynomial (or monomial) functions, the m_i are monomial functions, and $\mathbf{x} \in \mathbb{R}_{++}^n$ are the decision variables.

Although this form may appear restrictive, surprisingly many physical constraints and objectives can be expressed in the necessary form [1]. Many relationships that cannot be formulated exactly as posynomials can be approximated closely, using methods for fitting GP-compatible models to data [10].

B. Introduction to Signomial Programming

Geometric programming is a powerful tool, with strong guarantees. As discussed previously however, the formulation can prove restrictive. While changes of variable present an elegant way of circumventing some formulation obstacles, there may not always exist a suitable variable change. In particular, the restriction $c > 0$ in the definition of a posynomial can be a prohibitive obstacle for a modeler. There are many models where being able to use negative coefficients is necessary to accurately capture a relationship, such as when trying to minimize the difference between two quantities. An example of this is Lock's empirical relationship for wave drag [11] that is commonly used in conjunction with the Korn equation to estimate the drag on a transonic wing.

$$C_{D_{\text{wave}}} \geq 20(M - M_{\text{crit}})^4 \quad (4)$$

A *signomial* is a function with the same form as a posynomial,

$$s(\mathbf{x}) = \sum_{k=1}^K c_k \prod_{j=1}^n x_j^{a_{jk}}, \quad (5)$$

except that the coefficients, $c_k \in \mathbb{R}$, can now be any real number. In particular, they can be non-positive. A *signomial program* is a generalization of a geometric program that allows signomial constraints. The 'difference of convex' formulation of a signomial program also permits the objective function to be a ratio of posynomials and is given by:

$$\begin{aligned} & \text{minimize} \quad \frac{p_0(\mathbf{x})}{q_0(\mathbf{x})} \\ & \text{subject to} \quad s_i(\mathbf{x}) \leq 0, \quad i = 1, \dots, n_s, \\ & \quad \quad \quad p_j(\mathbf{x}) \leq 1, \quad j = 1, \dots, n_p, \\ & \quad \quad \quad m_k(\mathbf{x}) = 1, \quad k = 1, \dots, n_m. \end{aligned} \quad (6)$$

Although (6) is standard form for a signomial program, the majority of signomial constraints presented in this work take the form $p_1(\mathbf{x}) \leq p_2(\mathbf{x})$ or $s(\mathbf{x}) \leq p(\mathbf{x})$, because these are often more intuitive, and both can easily be transformed into the standard form $s(\mathbf{x}) \leq 0$. This follows the geometric programming convention of using posynomial inequality constraints of the form $p(\mathbf{x}) \leq m(\mathbf{x})$ and monomial equality constraints of the form $m_1(\mathbf{x}) = m_2(\mathbf{x})$ [2].

Sometimes there is both upward and downward (optimization) pressure on a variable and it is not always possible to know a priori which will dominate. In these cases, we can use signomial *equality* constraints of the form $s(\mathbf{x}) = 0$. However, as discussed in the next section, these constraints are generally less desirable than signomial inequality constraints from an optimization perspective. We therefore use them as sparingly as possible in this work.

An important point is that *adding just one signomial constraint to a geometric program with arbitrarily many posynomial constraints changes the geometric program to a signomial program*.

The bad news is that the increased expressiveness of signomial programming comes at a price: we can no longer guarantee a *global* optimum, because, unlike with GP, the log transformation of a signomial program is not a convex optimization problem. The good news is that there is a disciplined method for solving Signomial Programs (SPs).

C. Signomial Programming Solution Methods

There are a number of different methods for solving SPs. The majority of heuristics involve finding a local GP approximation to the SP about an initial guess, \mathbf{x}^0 , solving this GP, and then repeating the process, using the previous iteration's optimal solution as the point about which to take the next GP approximation. The process is repeated until the solution converges [2, 12]. The GP approximation is obtained by approximating each signomial constraint with a posynomial constraint.

The first step, if it has not already been done, is to express each signomial, $s_i(\mathbf{x})$, as a difference of posynomials, $p_i(\mathbf{x})$ and $q_i(\mathbf{x})$, and rearrange them to the form of a posynomial less than or equal to another posynomial.

$$s_i(\mathbf{x}) \leq 0 \quad (7)$$

$$p_i(\mathbf{x}) - q_i(\mathbf{x}) \leq 0 \quad (8)$$

$$p_i(\mathbf{x}) \leq q_i(\mathbf{x}) \quad (9)$$

Although (9) is not a GP-compatible constraint, it can be made into a GP constraint if posynomial $q_i(\mathbf{x})$ is replaced with its local monomial approximation, $\hat{q}_i(\mathbf{x}; \mathbf{x}^0)$, because a posynomial divided by a monomial is also a posynomial.

$$p_i(\mathbf{x}) \leq \hat{q}_i(\mathbf{x}; \mathbf{x}^0) \quad (10)$$

$$\frac{p_i(\mathbf{x})}{\hat{q}_i(\mathbf{x}; \mathbf{x}^0)} \leq 1 \quad (11)$$

Finding a monomial approximation to a posynomial is equivalent to finding a local affine approximation to a non-linear function in log space. The best-possible local monomial approximation to a posynomial $q(\mathbf{x})$ at the point \mathbf{x}^0 is given by [2]:

$$\hat{q}_i(\mathbf{x})|_{\mathbf{x}^0} = q_i(\mathbf{x}^0) \prod_{n=1}^N \left(\frac{x_n}{x_n^0} \right)^{a_n} \quad (12)$$

where x_n are the elements of \mathbf{x} and:

$$a_n = \frac{x_n^0}{q_i(\mathbf{x}^0)} \frac{\partial q_i}{\partial x_n}. \quad (13)$$

Signomial programming, using formulation (6), is an example of ‘difference of convex’ programming, because the logarithmically-transformed problem can be expressed as

$$\begin{aligned} &\text{minimize} && f_0(\mathbf{x}) - g_0(\mathbf{x}) \\ &\text{subject to} && f_i(\mathbf{x}) - g_i(\mathbf{x}) \leq 0, \quad i = 1, \dots, m \end{aligned} \quad (14)$$

where f_i and g_i are convex. This means that, for the convex (GP) approximation, $\hat{f}(\mathbf{x})$, of the non-convex (SP) function, $f(\mathbf{x}) - g(\mathbf{x})$,

$$\hat{f}(\mathbf{x}) \geq f(\mathbf{x}) \quad \forall \mathbf{x}. \quad (15)$$

Because of this, the true feasible set contains the feasible set of the convexified problem, and there is no need for a trust region [13], meaning that there is no need to tune solver parameters for controlling initial trust region sizes and/or update rules.

Signomial equality constraints are solved by creating local monomial approximations to the equality constraint. Unfortunately, the feasible set of the monomial approximation is not a subset of the original feasible set. Therefore, signomial equality constraints may require a trust region, making them the least desirable type of constraint. However, the signomial equality constraints in this work did not require a trust region, and thus, parameter tuning was not necessary. For additional details on how signomial equalities are implemented, see Opgenoord et al. [14]

The models solved in this paper employ a relaxed constants penalty function heuristic. This heuristic is a minor variation on the penalty convex-concave procedure described by Lipp and Boyd [12]. The heuristic employs the previously discussed iterative process, however, every constant in the model, c_i , is paired with a relaxed constant, \tilde{c}_i . Slack variables, s_i are introduced to facilitate the variation of the relaxed constants in accordance with Equations 16 through 18.

$$s_i \geq 1 \quad (16)$$

$$c_i \geq \frac{\tilde{c}_i}{s_i} \quad (17)$$

$$c_i \leq \tilde{c}_i s_i \quad (18)$$

The original objective function for each individual GP, $f(x)$, is modified to give a new objective function, $g(x)$, that heavily penalizes slack variables greater than one.

$$g(x) = \left(\sum s \right)^{20} f(x) \quad (19)$$

The large penalty on slack in the objective function ensures slack variables equal one when the SP converges. In other words, when the relaxed SP converges it is identical to the original model. The introduction of slack variables is advantageous because it allows early GP iterations to move through regions that are infeasible in the original model, reducing solution time while increasing model stability. It was observed in practice that the relaxed constants penalty method used in this paper was faster than the penalty convex concave procedure detailed in [12] because it involved introducing fewer additional variables, allowing the model to build faster.

The models presented in this work are composed and solved using Gpkit [15], a python package for defining and manipulating geometric programming models, with MOSEK [16] as the backend solver.

II. System-level Model

The objective of the optimization problem presented in this work is to minimize fuel consumption, or equivalently fuel weight, W_{fuel} , using an adaptation of the Breguet range formulation introduced in [1]. The purpose of the system-level model is threefold: it enforces system-level performance constraints such as required range and minimum cruise speed, it encodes weight and drag buildups,

and it constrains system-level properties such as the aircraft's Center of Gravity (CG) and moment of inertia. In doing these things, it also couples the subsystem models.

A. Model Assumptions

The model presented in this work is a set of constraints that describe the performance and design of a conventional-configuration narrowbody aircraft, with a simple cruise-only mission profile. A more sophisticated mission profile is left for future work.

B. Model Description

Table 1: Free variables in the system-level aircraft model and/or shared by sub-models

Free Variables	Units	Description
C_D	[-]	Drag coefficient
D	[N]	Total aircraft drag (cruise)
D_{fuse}	[N]	Fuselage drag
D_{ht}	[N]	Horizontal tail drag
D_{vt}	[N]	Vertical tail drag
D_{wing}	[N]	Wing drag
Δx_{ac_w}	[m]	Wing aerodynamic center shift
f_{fuel}	[-]	Percent fuel remaining
$I_{z_{fuse}}$	[kgm ²]	Fuselage moment of inertia
$I_{z_{tail}}$	[kgm ²]	Tail moment of inertia
$I_{z_{wing}}$	[kgm ²]	Wing moment of inertia
I_z	[kgm ²]	Total aircraft moment of inertia
l_{fuse}	[m]	Fuselage length
l_{vt}	[m]	Vertical tail moment arm
M	[-]	Cruise Mach number
R	[nm]	Segment range
S_w	[m ²]	Wing reference area
V_{TO}	[$\frac{m}{s}$]	Takeoff velocity
V_∞	[$\frac{m}{s}$]	Cruise velocity
W	[lbf]	Aircraft takeoff weight
W_{avg}	[lbf]	Flight segment average aircraft weight
W_{buoy}	[lbf]	Buoyancy weight
W_{dry}	[lbf]	Aircraft dry weight
W_{end}	[lbf]	Aircraft weight at end of flight segment
W_{fuel}	[lbf]	Fuel weight
$W_{fuel_{primary}}$	[lbf]	Total fuel weight less reserves
$W_{fuel_{wing}}$	[lbf]	Maximum fuel weight carried in wing
W_{fuse}	[lbf]	Fuselage weight
W_{hpesys}	[lbf]	Power system weight
W_{ht}	[lbf]	Horizontal tail weight
W_{lg}	[lbf]	Landing gear weight
W_{misc}	[lbf]	Miscellaneous system weight
W_{mg}	[lbf]	Main landing gear weight
W_{ng}	[lbf]	Nose landing gear weight
W_{pay}	[lbf]	Payload weight

W_{start}	[lbf]	Aircraft weight at start of flight segment
W_{tail}	[lbf]	Total tail weight
W_{vt}	[lbf]	Vertical tail weight
W_{wing}	[lbf]	Wing weight
W_{zf}	[lbf]	Zero fuel weight
\mathcal{R}_w	[-]	Wing aspect ratio
$\left(\frac{L}{D}\right)$	[-]	Lift/drag ratio
ξ	[-]	Takeoff parameter
a	$\left[\frac{m}{s}\right]$	Speed of sound
b_w	[m]	Wing span
c_{root_w}	[m]	Wing root chord
t	[min]	Flight time
x_{CG}	[m]	x-location of CG
$x_{CG_{lg}}$	[m]	x-location of landing gear CG
$x_{CG_{misc}}$	[m]	x-location of miscellaneous systems CG
x_{TO}	[m]	Takeoff distance
x_b	[m]	Wing box forward bulkhead location
x_{misc}	[m]	Miscellaneous systems centroid
x_{hpesys}	[m]	Power systems centroid
x_{lg}	[m]	Landing gear centroid
x_{mg}	[m]	Main landing gear centroid
x_{ng}	[m]	Nose landing gear centroid
x_{tail}	[m]	Tail centroid
x_{wing}	[m]	Wing centroid
y	[-]	Takeoff parameter
z_{bre}	[-]	Breguet parameter

Table 2: Fixed variables in the system-level aircraft model and/or shared by sub-models

Constants	Units	Description
$C_{L_{w,max}}$	[-]	Max lift coefficient, wing
M_{min}	[-]	Minimum Mach number
R_{req}	[nm]	Required total range
T_e	[N]	Takeoff thrust
W_{apu}	[N]	APU weight
W_{eng}	[N]	Engine weight
ρ_{TO}	$\left[\frac{kg}{m^3}\right]$	Takeoff density
c_T	$\left[\frac{lb}{(hr \cdot lb)}\right]$	Thrust specific fuel consumption
$f_{fuel_{res}}$	[-]	Fuel reserve fraction
g	$\left[\frac{m}{s^2}\right]$	Gravitational acceleration
h	[m]	Cruise altitude
l_r	[-]	Max Runway length
n_{eng}	[-]	number of engines
y_{eng}	[m]	Engine moment arm

1. Flight Performance

The Breguet range formulation is discretized over multiple cruise segments to improve accuracy, meaning the constraints from [1] apply during each of the N flight segments. The n subscript is used to represent the n^{th} flight segment where $n = 1...N$. For readability, these subscripts are not

used in the remainder of the manuscript, but still apply.

$$\sum_{n=1}^N R_n \geq R_{req} \quad (20)$$

$$R_{n+1} = R_n \quad (21)$$

$$R_n \leq \frac{V_{\infty_n}}{n_{eng} c_{T_n} g} \frac{W_{avg_n}}{D_n} z_{bre_n} \quad (22)$$

$$W_{fuel_n} \geq \left(z_{bre_n} + \frac{z_{bre_n}^2}{2} + \frac{z_{bre_n}^3}{6} \right) W_{end_n} \quad (23)$$

$$W_{fuel_n} \geq n_{eng} c_{T_n} D_n t_n \quad (24)$$

$$\sum_{n=1}^N W_{fuel_n} \leq W_{f_{primary}} \quad (25)$$

$$V_{\infty_n} t_n = R_n \quad (26)$$

$$W_{start_n} \geq W_{end_n} + W_{fuel_n} \quad (27)$$

$$W_{start_{n+1}} = W_{end_n} \quad (28)$$

$$W \geq W_{dry} + W_{payload} + f_{fuel_{res}} W_{f_{primary}} \quad (29)$$

$$W_{start_0} = W \quad (30)$$

$$W_{end_N} \geq W_{dry} + W_{payload} + f_{fuel_{res}} W_{f_{primary}} \quad (31)$$

$$W_{avg_n} \geq \sqrt{W_{start_n} W_{end_N}} + W_{buoy_n} \quad (32)$$

$$\left(\frac{L}{D} \right)_n = \frac{W_{avg_n}}{D_n} \quad (33)$$

In the remainder of this manuscript, W refers to the corresponding flight segment's W_{avg} .

The dry weight and drag of the aircraft are constrained using simple buildups of each component's weight and drag.

$$W_{dry} \geq W_{wing} + W_{fuse} + W_{vt} + W_{ht} + W_{lg} + W_{eng} + W_{misc} \quad (34)$$

$$D_n \geq D_{wing_n} + D_{fuse_n} + D_{vt_n} + D_{ht_n} \quad (35)$$

Mach number is constrained to be greater than a user-specified minimum value.

$$M = \frac{V_{\infty}}{a} \quad (36)$$

$$M \geq M_{min} \quad (37)$$

The takeoff model is taken directly from [1]. An additional constraint on takeoff velocity is added to ensure adequate margin above stall speed [17].

$$x_{TO} \leq l_r \quad (38)$$

$$1 + y \leq 2 \frac{g x_{TO} T_e}{V_{TO}^2 W} \quad (39)$$

$$1 \geq 0.0464 \frac{\xi^{2.7}}{y^{2.9}} + \frac{\xi^{0.3}}{y^{0.049}} \quad (40)$$

$$\xi \geq \frac{1}{2} \frac{\rho_{TO} V_{TO}^2 S_w C_D}{T_e} \quad (41)$$

$$V_{TO} = 1.2 \sqrt{\frac{2W}{C_{L_{w,max}} S_w \rho_{TO}}} \quad (42)$$

Atmospheric pressure, density, temperature, and speed of sound are constrained using the atmosphere model described in [18]. Dynamic viscosity is constrained using the viscosity model developed in [19] which is based off the Sutherland viscosity model [20].

2. System-level Properties

The constraint for the aircraft CG is GP-compatible, and is satisfied during each flight segment. The fuselage and payload weights are assumed to be evenly distributed through the length of the fuselage, and the wing weight acts directly at its area centroid, $x_{wing} + \Delta x_{ac_w}$. It is assumed that the fuel weight shifts in proportion to the remaining fuel fraction, f_{fuel} , and that a reserve fuel fraction, $f_{fuel_{res}}$, remains in the wing. The wingbox forward bulkhead location, x_b , is used as a surrogate variable for engine CG.

$$\begin{aligned} W x_{CG_n} \geq & W_{wing} (x_{wing} + \Delta x_{ac_w}) + W_{f_{primary}} (f_{fuel_n} + f_{fuel_{res}}) (x_{wing} + \Delta x_{ac_w} f_{fuel_n}) \\ & + \frac{1}{2} (W_{fuse} + W_{payload}) l_{fuse} + W_{ht} x_{CG_{ht}} + (W_{vt} + W_{cone}) x_{CG_{vt}} \\ & + n_{eng} W_{eng} x_b + W_{lg} x_{lg} + W_{misc} x_{misc} \end{aligned} \quad (43)$$

In the prior constraint, f_{fuel} is the percent of primary fuel remaining. f_{fuel} is represented adequately by a posynomial inequality since it has downward pressure.

$$f_{fuel_n} \geq \frac{\sum_{n=1}^n W_{fuel_n}}{W_{f_{primary}}} \quad (44)$$

The landing gear CG is constrained by the moment of each set of landing gear about the nose of the aircraft.

$$W_{lg} x_{lg} \geq W_{mg} x_m + W_{ng} x_n \quad (45)$$

The miscellaneous equipment CG includes only power systems in the current model, but is defined to allow for refinements in CG modeling in future work.

$$W_{misc} x_{misc} \geq W_{hpesys} x_{hpesys} \quad (46)$$

The aircraft's moment of inertia is the sum of the inertias of its components.

$$I_z \geq I_{z_{wing}} + I_{z_{fuse}} + I_{z_{tail}} \quad (47)$$

The wing moment of inertia model includes the moment of inertia of the fuel systems and engines. It assumes that the wing and fuel weight are evenly distributed on the planform of the wing. This is an overestimate of the wing moment of inertia with full fuel tanks.

$$I_{z_{wing}} \geq \frac{n_{eng} W_{engine} y_{eng}^2}{g} + \left(\frac{W_{fuel_{wing}} + W_{wing}}{g} \right) \frac{b_w^3 c_{root_w}}{16 S_w} \left(\lambda_w + \frac{1}{3} \right) \quad (48)$$

The fuselage moment of inertia includes the payload moment of inertia. It is assumed that payload and fuselage weight are evenly distributed along the length of the fuselage. The wing root quarter-chord location acts as a surrogate for the CG of the aircraft.

$$I_{z_{fuse}} \geq \left(\frac{W_{fuse} + W_{pay}}{g} \right) \left(\frac{x_{wing}^3 + l_{vt}^3}{3l_{fuse}} \right) \quad (49)$$

The moment of inertia of the tail is constrained by treating the tail as a point mass.

$$I_{z_{tail}} \geq \left(\frac{W_{apu} + W_{tail}}{g} \right) l_{vt}^2 \quad (50)$$

III. Wing Model

The overarching purpose of an aircraft wing is to generate sufficient lift such that the aircraft can takeoff, climb, cruise, descend, and land safely. Typically the wings also carry fuel tanks and support the engines. Unfortunately, wings are heavy and produced drag. The purpose of this model is to relate all of these considerations.

A. Model Assumptions

The wing model assumes a continuous-taper, low-wing configuration with a modern transonic airfoil. It does not currently consider wing twist or wing dihedral. It also does not consider roll or yaw stability.

B. Model Description

The wing model has 52 free variables and 49 constraints.

Table 3: Free variables in the wing model

Free Variables	Units	Description
\mathcal{R}_w	[-]	Wing aspect ratio
C_{D_w}	[-]	Drag coefficient, wing
$C_{D_{iw}}$	[-]	Wing induced drag coefficient
$C_{D_{pw}}$	[-]	Wing parasitic drag coefficient
C_{L_w}	[-]	Lift coefficient, wing
$C_{L_{\alpha-w}}$	[-]	Lift curve slope, wing
D_w	[N]	Wing drag
L_w	[N]	Wing lift
L_{ht}	[N]	Horizontal tail downforce
$L_{w_{max}}$	[m]	Max lift generated by wing
L_{total}	[N]	Total lift generated by aircraft
M	[-]	Cruise Mach number
Re_w	[-]	Cruise Reynolds number (wing)
S_w	[m ²]	Wing area
V_∞	[$\frac{m}{s}$]	Freestream velocity
$V_{fuel,max}$	[m ³]	Available fuel volume
W	[lbf]	Aircraft weight

W_S	$[\frac{N}{m^2}]$	Wing loading
$W_{fuel_{total}}$	[lbf]	Total fuel weight
W_{fuel}	[lbf]	Fuel weight on aircraft at any point in flight
W_{struct_w}	[lbf]	Wing box weight
W_{total}	[lbf]	Aircraft max weight
W_{wing}	[lbf]	Wing weight
ΔL_o	N	Center wing lift loss
ΔL_t	N	Wing tip lift loss
Δx_{ac_w}	N	Wing aerodynamic center shift
α_w	[-]	Wing angle of attack
\bar{c}_w	[m]	Mean aerodynamic chord (wing)
η_o	[-]	Center wing span coefficient
λ_w	[-]	Wing taper ratio
μ	$[\frac{N \cdot s}{m^2}]$	Dynamic viscosity
ρ_∞	$[\frac{kg}{m^3}]$	Freestream density
τ_w	[-]	Wing thickness/chord ratio
b_w	[m]	Wing span
c_{root_w}	[m]	Wing root chord
c_{tip_w}	[m]	Wing tip chord
e	[-]	Oswald efficiency factor
$f(\lambda_w)$	[-]	Empirical efficiency function of taper
p_w	[-]	Substituted variable = $1 + 2 \cdot \text{taper}$
p_o	$\frac{N}{m}$	Center section theoretical wing loading
q_w	[-]	Substituted variable = $1 + \text{taper}$
$y\bar{c}_w$	[m]	Spanwise location of mean aerodynamic chord

WingBox

I_{cap}	[-]	Non-dim spar cap area moment of inertia
$L_{ht_{max}}$	[N]	Maximum horizontal tail downforce
M_r	[N]	Root moment per root chord
W_{cap}	[lbf]	Weight of spar caps
$W_{fuel_{wing}}$	[lbf]	Maximum fuel weight carried in wing
W_{web}	[lbf]	Weight of shear web
ν	[-]	Dummy variable = $(t^2 + t + 1)/(t + 1)^2$
t_{cap}	[-]	Non-dim. spar cap thickness
t_{web}	[-]	Non-dim. shear web thickness

Table 4: Fixed variables in the wing model

Constants	Units	Description
$C_{L_{w,max}}$	[-]	Max lift coefficient, wing
$\alpha_{w,max}$	[-]	Max angle of attack
$\cos(\Lambda)$	[-]	Cosine of quarter-chord sweep angle
η_w	[-]	Lift efficiency (diff b/w sectional, actual lift)
$\lambda_{w,min}$	[-]	Minimum wing taper ratio
ρ_{fuel}	$[\frac{kg}{m^3}]$	Density of fuel
$\tan(\Lambda)$	[-]	Tangent of quarter-chord sweep angle
$b_{w,max}$	[m]	Max allowed wingspan
f_{L_o}	[-]	Center wing lift reduction coefficient
$f_{L_{total}/wing}$	[-]	Total lift divided by wing lift
f_{L_t}	[-]	Wing tip lift reduction coefficient
$f_{aileron}$	[-]	Aileron added weight fraction

f_{flap}	[-]	Flap added weight fraction
$f_{fuel,usable}$	[-]	Usability factor of max fuel volume
$f_{fuel,wing}$	[-]	Fraction of total fuel stored in wing
f_{lete}	[-]	Lete added weight fraction
f_{ribs}	[-]	Wing rib added weight fraction
f_{slat}	[-]	Slat added weight fraction
$f_{spoiler}$	[-]	Spoiler added weight fraction
f_{tip}	[-]	Induced drag reduction from wing tip devices
f_{watt}	[-]	Watt added weight fraction
g	$[\frac{m}{s^2}]$	Gravitational acceleration
y_{eng}	[m]	Engine moment arm
W_{engine}	[N]	Engine weight
$W_{S_{max}}$	$[\frac{N}{m^2}]$	Maximum wing loading

WingBox

N_{lift}	[-]	Wing loading multiplier
ρ_{cap}	$[\frac{kg}{m^3}]$	Density of spar cap material
ρ_{web}	$[\frac{kg}{m^3}]$	Density of shear web material
$\sigma_{max,shear}$	[Pa]	Allowable shear stress
σ_{max}	[Pa]	Allowable tensile stress
r_h	[-]	Fractional wing thickness at spar web
w	[-]	Wingbox-width-to-chord ratio

1. Wing Geometry

Before considering a wing's performance, the variables that prescribe its geometry must be appropriately constrained.

The relationship between reference area, span and mean geometric chord is enforced using a constraint that assumes a trapezoidal planform. This constraint is implemented as a signomial equality constraint because there is both upward and downward (optimization) pressure on the reference area, and it is not possible to know a priori which will dominate.

$$S_w = b_w \frac{c_{root_w} + c_{tip_w}}{2} \quad (51)$$

The mean aerodynamic chord relationship for a trapezoidal wing can be written as a signomial constraint, and its spanwise location can be written as a monomial equality constraint. These constraints make use of dummy variables, p_w and q_w , introduced by the structural model below.

$$\bar{c}_w \leq \frac{2}{3} \left(\frac{1 + \lambda_w + \lambda_w^2}{q_w} \right) c_{root_w} \quad (52)$$

$$y_{\bar{c}_w} = \frac{b_w q_w}{3 p_w} \quad (53)$$

The wing taper ratio is defined by a monomial equality constraint. It is necessary to lower bound taper to avoid an unacceptably small Reynolds number at the wing tip [22]. For the purpose of this work, the taper is lower bounded using the taper ratio of the reference aircraft's wing [23].

$$\lambda_w = \frac{c_{tip_w}}{c_{root_w}} \quad (54)$$

^bGeometric in the sense that they prescribe geometry, not in the sense of geometric programming, which derives its name from the same etymology as the geometric mean.

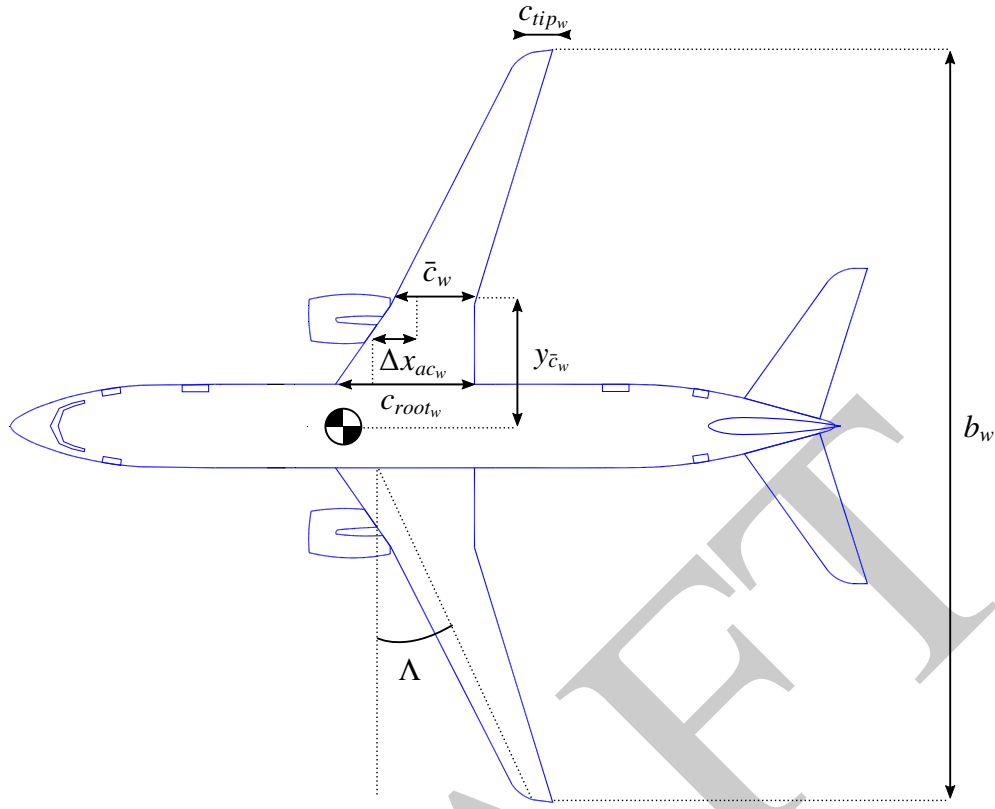


Figure 1: Geometric variables^b of the wing model (adapted from [21])

$$\lambda_w \geq \lambda_{wmin} \quad (55)$$

Finally, a maximum span constraint can be imposed to reflect, for example, a gate size constraint.

$$b_w \leq b_{w,max} \quad (56)$$

2. Wing Lift

Total lift is constrained to be greater than the weight of the aircraft plus the downforce from the horizontal tail. The constant $f_{L_{total}/wing}$ is greater than one and used to account for fuselage lift.

$$L_{total} \geq W + L_{ht} \quad (57)$$

$$L_{total} = f_{L_{total}/wing} L_w \quad (58)$$

The standard equation for the lift of a wing is a natural monomial equality constraint.

$$L_w = \frac{1}{2} \rho_\infty V_\infty^2 S_w C_{L_w} \quad (59)$$

However, this assumes a continuous unobstructed wing planform. Correcting for lift loss at the fuselage and at the wing tips, gives the adjusted Equation (60), which can be rearranged into the

posynomial Constraint (61).

$$L_w = \frac{1}{2}\rho_\infty V_\infty^2 S_w C_{L_w} - \Delta L_o - 2\Delta L_t \quad (60)$$

$$\frac{1}{2}\rho_\infty V_\infty^2 S_w C_{L_w} \geq L_w + \Delta L_o + 2\Delta L_t \quad (61)$$

The lift corrections are given as monomial equality constraints [5].

$$\Delta L_o = \eta_o f_{L_o} \frac{b_w}{2} p_o \quad (62)$$

$$\Delta L_t = f_{L_t} p_o c_{root_w} \lambda_w^2 \quad (63)$$

The lift coefficient of the wing goes linearly with the angle of attack, which is limited by a maximum angle of attack due to stall.

$$C_{L_w} = C_{L_{\alpha,w}} \alpha_w \quad (64)$$

$$\alpha_w \leq \alpha_{w,max} \quad (65)$$

The DATCOM formula is an analytic function for estimating the lift curve slope of a wing or tail, based on empirical results [22].

$$C_{L_{\alpha,w}} = \frac{2\pi \mathcal{R}_w}{2 + \sqrt{(\mathcal{R}_w/\eta_w)^2(1 + \tan^2 \Lambda - M^2) + 4}} \quad (66)$$

This relationship can be used as a signomial inequality to constrain the lift curve slope, although some algebraic manipulation is needed.

$$C_{L_{\alpha,w}} \leq \frac{2\pi \mathcal{R}_w}{2 + \sqrt{(\mathcal{R}_w/\eta_w)^2(1 + \tan^2 \Lambda - M^2) + 4}} \quad (67)$$

$$(\mathcal{R}_w/\eta_w)^2(1 + \tan^2 \Lambda - M^2) + 4 \leq \left(\frac{2\pi \mathcal{R}_w}{C_{L_{\alpha,w}}} - 2 \right)^2 \quad (68)$$

$$(\mathcal{R}_w/\eta_w)^2(1 + \tan^2 \Lambda - M^2) \leq \frac{4\pi^2 \mathcal{R}_w^2}{C_{L_{\alpha,w}}^2} - \frac{8\pi \mathcal{R}_w}{C_{L_{\alpha,w}}} \quad (69)$$

$$\frac{C_{L_{\alpha,w}}^2}{\eta_w^2} (1 + \tan^2 \Lambda - M^2) + \frac{8\pi C_{L_{\alpha,w}}}{\mathcal{R}_w} \leq 4\pi^2 \quad (70)$$

Maximum wing lift is constrained using an assumed load factor, N_{lift} .

$$f_{L_{total}/wing} L_{w,max} \geq N_{lift} W_{total} + L_{ht,max} \quad (71)$$

Finally, wing loading is constrained to be less than a user specified maximum.

$$W_S = \frac{1}{2}\rho_\infty C_{L_w} V_\infty^2 \quad (72)$$

$$W_S \leq W_{S,max} \quad (73)$$

3. Wing Weight

Wing weight is constrained to be greater than the wing structural weight plus a series of fractional weights to account for wing ribs and control surfaces.

$$W_{wing} \geq W_{struct_w}(1 + f_{flap} + f_{slat} + f_{aileron} + f_{lete} + f_{ribs} + f_{spoiler} + f_{watt}) \quad (74)$$

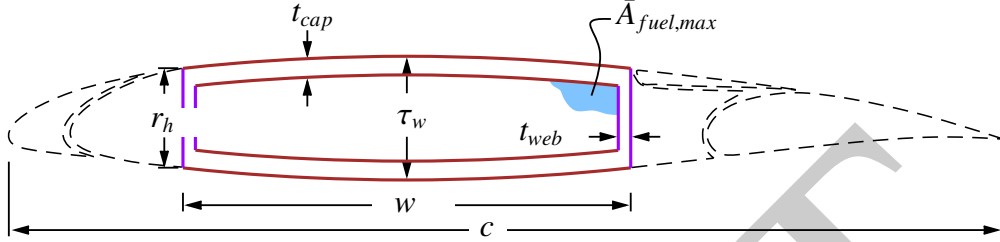


Figure 2: Geometric variables of the wingbox cross-section (adapted from [5])

Wing structural weight is constrained using an adaptation of the structural model from Hoburg [1], which comprises 12 monomial and posynomial constraints.

$$W_{struct_w} \geq (W_{cap} + W_{web}) \quad (75)$$

$$W_{cap} \geq \frac{8\rho_{cap}gwt_{cap}S_w^{1.5}\nu}{3\mathcal{R}_w^{0.5}} \quad (76)$$

$$W_{web} \geq \frac{8\rho_{web}gr_h\tau_w t_{web}S_w^{1.5}\nu}{3\mathcal{R}_w^{0.5}} \quad (77)$$

$$\nu^{3.94} \geq 0.14p_w^{0.56} + \frac{0.86}{p_w^{2.4}} \quad (78)$$

$$p_w \geq 1 + 2\lambda_w \quad (79)$$

$$2q_w \geq 1 + p_w \quad (80)$$

$$\frac{0.92^2}{2}\tau_w^2 t_{cap}w \geq 0.92\tau_w t_{cap}^2w + I_{cap} \quad (81)$$

$$\frac{\mathcal{R}_w M_r N_{lift} \tau_w q_w^2}{I_{cap} S_w \sigma_{max}} \leq 8 \quad (82)$$

$$\frac{\mathcal{R}_w L_{w_{max}} N_{lift} q_w^2}{S_w \sigma_{max, shear} \tau_w t_{web}} \leq 12 \quad (83)$$

$$\mathcal{R}_w = \frac{b_w^2}{S_w} \quad (84)$$

$$\tau_w \leq 0.14 \quad (85)$$

The original root bending moment constraint,

$$M_r \geq \frac{\mathcal{R}_w L_{w_{max}} p_w}{24}, \quad (86)$$

is replaced with a more sophisticated signomial constraint that considers the load relief effect due to the weight of the engine and the fuel tanks. To derive the constraint, the lift per unit span of

wing is assumed to be proportional to the local chord, and the wing planform area is partitioned into an untapered (rectangular) area A_{rect} and a fully tapered (triangular) area A_{tri} .

$$A_{tri} = \frac{1}{2}(1 - \lambda_w)c_{root_w}b_w \quad (87)$$

$$A_{rect} = c_{tip_w}b_w \quad (88)$$

The wing area component loads are treated as point loads to determine the equivalent wing root moment.

$$M_r c_{root_w} \geq \left(L_{w_{max}} - N_{lift} (W_{wing} + f_{fuel,wing} W_{fuel}) \right) \left(\frac{1}{6} A_{tri} + \frac{1}{4} A_{rect} \right) \frac{b_w}{S_w} - N_{lift} W_{engine} y_{eng} \quad (89)$$

This constraint can be further simplified to remove the need for intermediary variables A_{tri} and A_{rect} , since

$$\frac{1}{6} A_{tri} + \frac{1}{4} A_{rect} = \frac{1}{12} (c_{root_w} - c_{tip_w}) b_w + \frac{1}{4} c_{tip_w} b_w \quad (90)$$

$$= \frac{b_w}{12} (c_{root_w} + 2c_{tip_w}). \quad (91)$$

Substituting Equation (91) into Constraint (89) yields the following wing root moment constraint.

$$M_r c_{root_w} \geq \left(L_{w_{max}} - N_{lift} (W_{wing} + f_{fuel,wing} W_{fuel}) \right) \left(\frac{b_w^2}{12 S_w} (c_{root_w} + 2c_{tip_w}) \right) - N_{lift} W_{engine} y_{eng} \quad (92)$$

Note that this provides a conservative estimate for the root moment, since it assumes that the lift per unit area is constant throughout the wing, whereas in reality the lift per unit area diminishes towards the wingtips.

4. Wing Drag

Wing drag is captured by five monomial and posynomial constraints. The parasitic drag coefficient is constrained using a softmax affine fit of XFOIL [24] simulation data for the TASOPT [5] C-series airfoils, which are representative of modern transonic airfoils [5]. The fit, which considers wing thickness, lift coefficient, Reynolds number, and Mach number, was developed with GPfit [10,25] and has an RMS error of approximately 5%. Constraint (97) is an adaption of the standard definition of the induced drag coefficient [17], with an adjustment factor for wingtip devices.

$$D_w = \frac{1}{2} \rho_\infty V_\infty^2 S_w C_{D_w} \quad (93)$$

$$C_{D_w} \geq C_{D_{pw}} + C_{D_{iw}} \quad (94)$$

$$C_{D_{pw}}^{1.65} \geq 1.61 \left(\frac{Re_w}{1000} \right)^{-0.550} (\tau_w)^{1.29} (M \cos(\Lambda))^{3.04} C_{L_w}^{1.78} + 0.0466 \left(\frac{Re_w}{1000} \right)^{-0.389} (\tau_w)^{0.784} (M \cos(\Lambda))^{-0.340} C_{L_w}^{0.951} \quad (95)$$

$$\begin{aligned}
& + 191 \left(\frac{Re_w}{1000} \right)^{-0.219} (\tau_w)^{3.95} (M \cos(\Lambda))^{19.3} C_{L_w}^{1.15} \\
& + 2.82e - 12 \left(\frac{Re_w}{1000} \right)^{1.18} (\tau_w)^{-1.76} (M \cos(\Lambda))^{0.105} C_{L_w}^{-1.44} \\
Re_w &= \frac{\rho_\infty V_\infty \bar{c}_w}{\mu}
\end{aligned} \tag{96}$$

$$C_{D_{i_w}} \geq f_{tip} \frac{C_{L_w}^2}{\pi e \mathcal{R}_w} \tag{97}$$

The Oswald efficiency is constrained by a relationship from [26], in which the authors fit a polynomial function to empirical data. Given that all polynomials are signomials, this can easily be used in the SP framework.

$$e \leq \frac{1}{1 + f(\lambda_w) \mathcal{R}_w} \tag{98}$$

$$f(\lambda_w) \geq 0.0524\lambda_w^4 - 0.15\lambda_w^3 + 0.1659\lambda_w^2 - 0.0706\lambda_w + 0.0119 \tag{99}$$

The Oswald efficiency is plotted as a function of taper ratio, as imposed by this pair of constraints, in Figure 3.

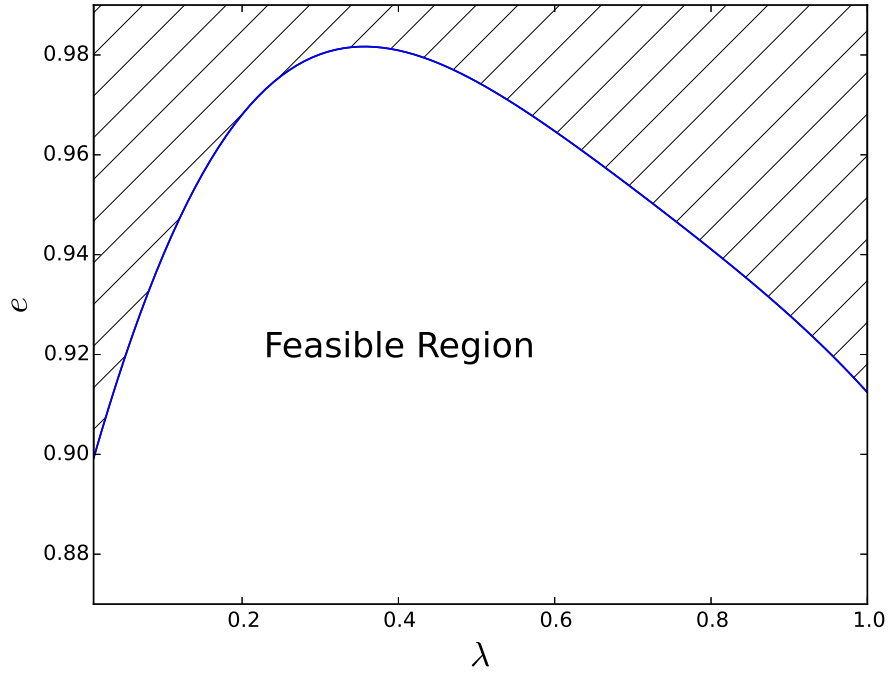


Figure 3: Empirical relationship for Oswald efficiency as a function of taper for a wing with $\mathcal{R}_w=10$

5. Wing Aerodynamic Center

The true aerodynamic center and the CG of the wing are shifted in the aircraft's x-axis with respect to the wing root quarter chord due to the swept geometry of the wing. This effect is captured with the variable Δx_{ac_w} . Assuming that the wing lift per unit area is constant, and by integrating the

product of the local quarter chord offset $\delta x(y)$ and local chord area $c(y)dy$ over the wing-half span, it can be calculated by

$$\Delta x_{ac_w} = \frac{2}{S} \int_0^{b/2} c(y) \delta x(y) dy, \quad (100)$$

where the local root chord $c(y)$ and the local quarter chord offset $\delta x(y)$ are given by:

$$c(y) = \left(1 - (1 - \lambda_w) \frac{2y}{b_w}\right) c_{root_w} \quad (101)$$

$$\delta x(y) = y \tan(\Lambda) \quad (102)$$

By substituting Equations (101) and (102) into Equation (100), expanding out the integral and relaxing the equality, Δx_{ac_w} can be constrained as follows.

$$\Delta x_{ac_w} \geq \frac{1}{4} \tan(\Lambda) R_w c_{root_w} \left(\frac{1}{3} + \frac{2}{3} \lambda_w\right) \quad (103)$$

6. Fuel Volume

Fuel tanks are typically located inside the wingbox. Using the geometry of a TASOPT-optimized 737-800 [5], a constraint on the maximum fuel volume in the wing was developed. For a wing of the same mean aerodynamic chord, thickness, and span as a TASOPT 737-800, the maximum available fuel volumes in the wing will match exactly. To allow for the possibility of auxiliary tanks in the horizontal tail or fuselage the user-specified value $f_{fuel,usable}$ is introduced.

$$V_{fuel,max} \leq 0.303 \bar{c}_w^2 b_w \tau_w \quad (104)$$

$$W_{fuel,wing} \leq \rho_{fuel} V_{fuel,max} g \quad (105)$$

$$W_{fuel,wing} \geq \frac{f_{fuel,wing} W_{fuel,total}}{f_{fuel,usable}} \quad (106)$$

IV. Vertical Tail Model

At a conceptual design level, the purpose of an aircraft's vertical tail is two-fold. Firstly, it must provide stability in yaw. Secondly, it must provide adequate yaw control authority in critical flight conditions. For a multi-engine aircraft, the critical flight condition is typically an engine failure at low speeds. The vertical tail must be capable of providing sufficient sideforce in this case [27]. The vertical tail must also provide adequate yaw rate acceleration during landing flare in crosswind conditions. The design of the vertical tail is therefore coupled to the size of the fuselage, the position of the engines, and the aircraft's moment of inertia.

A. Model Assumptions

The high-level assumptions for this model are that the horizontal tail is mounted on the fuselage, so as to not require a reinforced vertical tail structure, and that the aircraft has two engines.

B. Model Description

The vertical tail model has 42 free variables and 31 constraints.

Table 5: Free variables in the vertical tail model

DRAFT

Free Variables	Units	Description
\mathcal{R}_{vt}	[-]	Vertical tail aspect ratio
$C_{D_{pvt}}$	[-]	Viscous drag coefficient
$C_{L_{vt,EO}}$	[-]	Vertical tail lift coefficient during engine out
$C_{L_{vt,landing}}$	[-]	Vertical tail lift coefficient during landing
$C_{L_{vt}}$	[-]	Vertical tail lift coefficient
D_{vt}	[N]	Vertical tail viscous drag, cruise
D_{wm}	[N]	Engine out windmill drag
I_z	[kgm ²]	Total aircraft moment of inertia
$L_{vt,EO}$	[N]	Vertical tail lift in engine out
$L_{vt,max}$	[N]	Maximum load for structural sizing
M	[-]	Cruise Mach number
Re_{vt}	[-]	Vertical tail reynolds number
S_{vt}	[m ²]	Vertical tail reference area (half)
V_∞	[$\frac{m}{s}$]	Freestream velocity
W_{struct}	[lbf]	Full span weight
W_{vt}	[lbf]	Vertical tail weight
$\Delta x_{lead_{vt}}$	[m]	Distance from CG to VT leading edge
$\Delta x_{trail_{vt}}$	[m]	Distance from CG to VT trailing edge
\bar{c}_{vt}	[m]	Vertical tail mean aero chord
λ_{vt}	[-]	Vertical tail taper ratio
μ	[$\frac{N \cdot s}{m^2}$]	Dynamic viscosity
ρ_∞	[$\frac{kg}{m^3}$]	Freestream density
τ_{vt}	[-]	Vertical tail thickness/chord ratio
b_{vt}	[m]	Vertical tail half span
$c_{root_{vt}}$	[m]	Vertical tail root chord
$c_{tip_{vt}}$	[m]	Vertical tail tip chord
l_{fuse}	[m]	Length of fuselage
l_{vt}	[m]	Vertical tail moment arm
$x_{CG_{vt}}$	[m]	Location of vertical tail CG
x_{CG}	[m]	Location of aircraft CG
$z\bar{c}_{vt}$	[m]	Vertical location of mean aerodynamic chord

Table 6: Fixed variables in the vertical tail model

Constants	Units	Description
A_{fan}	[m ²]	Engine reference area
$C_{D_{wm}}$	[-]	Windmill drag coefficient
$C_{L_{vt,max}}$	[-]	Max lift coefficient
T_e	[N]	Thrust per engine at takeoff
V_1	[$\frac{m}{s}$]	Minimum takeoff velocity
V_{land}	[$\frac{m}{s}$]	Landing velocity
V_{ne}	[$\frac{m}{s}$]	Never exceed velocity
$\lambda_{vt,min}$	[-]	Minimum vertical tail taper ratio
ρ_{TO}	[$\frac{kg}{m^3}$]	Air density at takeoff
$\tan(\Lambda_{vt})$	[-]	Tangent of leading edge sweep (40 deg)
$c_{l_{vt,EO}}$	[-]	Sectional lift force coefficient (engine out)
e_{vt}	[-]	Span efficiency of vertical tail
g	[$\frac{m}{s^2}$]	Gravitational acceleration
\dot{r}_{req}	[s ⁻²]	Max required yaw rate acceleration at landing
y_{eng}	[m]	Engine moment arm

1. Vertical Tail Geometry and Structure

The variables that define geometry are illustrated in Figure 4. The moment arm of the vertical tail is the distance from the aircraft CG to the aerodynamic center of the vertical tail, which is assumed to be at the quarter chord. The moment arm is therefore upper bounded by the distance from the CG to the leading edge of the tail at the root, the height of the mean aerodynamic chord above the fuselage, the sweep angle, and the mean aerodynamic chord.

$$l_{vt} \leq \Delta x_{lead_{vt}} + z_{\bar{c}_{vt}} \tan(\Lambda_{LE}) + 0.25 \bar{c}_{vt} \quad (107)$$

The x-coordinates of the leading and trailing edge at the root are related by the root chord. The tail trailing edge is upper bounded by imposing a constraint that the tail root cannot extend beyond the end of the fuselage. Together these constraints put an upper bound on the moment arm of the tail based on the length of the fuselage.

$$\Delta x_{trail_{vt}} \geq \Delta x_{lead_{vt}} + c_{root_{vt}} \quad (108)$$

$$l_{fuse} \geq x_{CG} + \Delta x_{trail_{vt}} \quad (109)$$

The vertical tail structure is sized by its maximum lift coefficient and the never-exceed speed.

$$L_{vt_{max}} = \frac{1}{2} \rho_{TO} V_{ne}^2 S_{vt} C_{L_{v,max}} \quad (110)$$

The remaining geometry and structural constraints were already introduced in the wing model. Constraints (51) to (55) are adapted to the vertical tail model to constrain its geometry, with two minor modifications. Constraint (51) can be relaxed from a signomial equality to a signomial inequality constraint, meanwhile Constraint (52) needs to be implemented as a signomial equality constraint. The wing structure model from [1] is also reused, however, given that the vertical tail only has a half-span, the definitions of b_{vt} , S_{vt} , and W_{vt} differ from those of their wing counterparts.

2. Engine-out Condition

The first performance constraint specifies that the maximum moment exerted by the tail must be greater than or equal to the moment exerted by the engines in an engine-out condition, exacerbated by the windmill drag of the engine that is inoperative [5].

$$L_{vt,EO} l_{vt} \geq D_{wm} y_{eng} + T_e y_{eng} \quad (111)$$

The worst case engine out condition is likely to occur during takeoff, when the velocity is lowest but the engine force required to safely complete takeoff is highest. The force exerted by the vertical tail in this critical low speed case is constrained by its maximum lift coefficient, its reference area and the minimum dynamic pressure. As a conservative estimate, the V_1 speed is used because it is the minimum speed after which a takeoff can be completed, following a critical engine failure.

$$L_{vt,EO} = \frac{1}{2} \rho_{TO} V_1^2 S_{vt} C_{L_{vt,EO}} \quad (112)$$

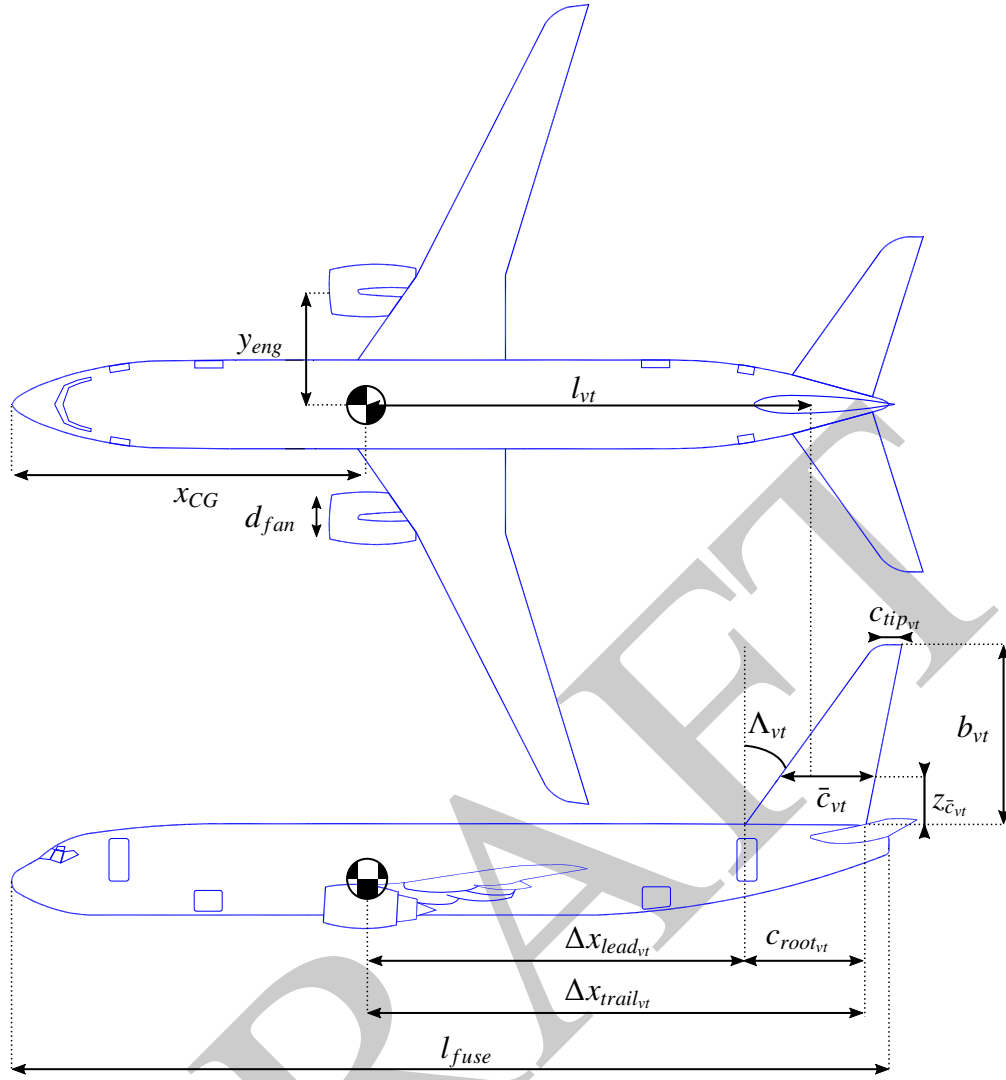


Figure 4: Geometric variables of the vertical tail model (adapted from [21])

The 3D lift coefficient is constrained by the airfoil sectional lift coefficient using finite wing theory [28].

$$C_{L_{vt,EO}} \left(1 + \frac{c_{l_{vt,EO}}}{\pi e_{vt} \mathcal{R}_{vt}} \right) \leq c_{l_{vt,EO}} \quad (113)$$

The windmill drag can, to a first approximation, be lower bounded using a drag coefficient and a reference area [5], in this case the area of the engine fan.

$$D_{wm} \geq \frac{1}{2} \rho_{TO} V_1^2 A_{fan} C_{D_{wm}} \quad (114)$$

3. Crosswind Landing Condition

The second performance constraint ensures the vertical tail can provide adequate yaw rate acceleration in a crosswind landing, where the moment of inertia was constrained at the system level (Section II). To provide a safety margin during cross-wind landing, $C_{L_{vt,landing}}$ is taken to be 85% of

takeoff $C_{L_{vt}}$.

$$\frac{1}{2}\rho_{TO}V_{land}^2S_{vt}l_{vt}C_{L_{vt,landing}} \geq \frac{\dot{r}_{req}}{I_z} \quad (115)$$

4. Vertical Tail Drag

The vertical tail produces drag, regardless of the flight condition. Neglecting any induced drag, the parasitic drag coefficient, $C_{D_{p_{vt}}}$, is set by a softmax affine fit of XFOIL [24] data for the symmetric NACA 0008 through 0020 airfoils. The fit considers airfoil thickness, Mach number, and Reynolds number. It was developed with GPfit [10, 25] and has an RMS error of 1.31%.

$$D_{vt} \geq \frac{1}{2}\rho_{\infty}V_{\infty}^2S_{vt}C_{D_{p_{vt}}} \quad (116)$$

$$C_{D_{p_{vt}}}^{1.189} \geq 2.44 \times 10^{-77}(Re_{vt})^{-0.528}(\tau_{vt})^{133.8}(M)^{1022.7} \\ + 0.003(Re_{vt})^{-0.410}(\tau_{vt})^{1.22}(M)^{1.55} \\ + 1.967 \times 10^{-4}(Re_{vt})^{0.214}(\tau_{vt})^{-0.04}(M)^{-0.14} \\ + 6.590 \times 10^{-50}(Re_{vt})^{-0.498}(\tau_{vt})^{1.56}(M)^{-114.6} \quad (117)$$

$$Re_{vt} = \frac{\rho_{\infty}V_{\infty}\bar{c}_{vt}}{\mu} \quad (118)$$

V. Horizontal Tail Model

At a conceptual design level, the purpose of the horizontal tail is threefold: to trim the aircraft such that it can fly in steady level flight, to provide longitudinal stability, and to give the pilot pitch control authority over a range of flight conditions.

A. Model Assumptions

The horizontal tail model assumes that the horizontal stabilizer is mounted to the fuselage and nominally produces downforce in cruise.

B. Model Description

The horizontal tail model has 50 free variables and 33 constraints.

Table 7: Free variables in the horizontal tail model

Free Variables	Units	Description
$C_{D_{ht}}$	[-]	Horizontal tail drag coefficient
$C_{D_{0_{ht}}}$	[-]	Horizontal tail parasitic drag coefficient
$C_{L_{ht}}$	[-]	Lift coefficient (htail)
C_{L_w}	[-]	Lift coefficient (wing)
$C_{L_{\alpha h_0}}$	[-]	Isolated lift curve slope (htail)
$C_{L_{\alpha,ht}}$	[-]	Lift curve slope (htail)
$C_{L_{\alpha,w}}$	[-]	Lift curve slope (wing)
D_{ht}	[N]	Horizontal tail drag
L_{ht}	[N]	Horizontal tail downforce

$L_{ht,max}$	[N]	Maximum tail load
M	[-]	Mach number
Re_{ht}	[-]	Horizontal tail Reynolds number
$S.M.$	[-]	Stability margin
S_{ht}	[m ²]	Horizontal tail area
V_{∞}	[$\frac{m}{s}$]	Freestream velocity
V_{ht}	[-]	Horizontal tail volume
W_{ht}	[lbf]	Horizontal tail weight
R_w	[-]	Wing aspect ratio
R_{ht}	[-]	Horizontal tail aspect ratio
$\Delta x_{lead_{ht}}$	[m]	Distance from CG to HT leading edge
$\Delta x_{trail_{ht}}$	[m]	Distance from CG to HT trailing edge
α_{ht}	[-]	Horizontal tail angle of attack
\bar{c}_w	[m]	Mean aerodynamic chord (wing)
\bar{c}_{ht}	[m]	Mean aerodynamic chord (ht)
λ_{ht}	[-]	Horizontal tail taper ratio
μ	[$\frac{N \cdot s}{m^2}$]	Dynamic viscosity
ρ_{∞}	[$\frac{kg}{m^3}$]	Freestream density
τ_{ht}	[-]	Horizontal tail thickness/chord ratio
b_{ht}	[m]	Horizontal tail span
$c_{root_{ht}}$	[m]	Horizontal tail root chord
$c_{tip_{ht}}$	[m]	Horizontal tail tip chord
e_{ht}	[-]	Oswald efficiency factor
$f(\lambda_{ht})$	[-]	Empirical efficiency function of taper
l_{fuse}	[m]	Fuselage length
l_{ht}	[m]	Horizontal tail moment arm
m_{ratio}	[-]	Ratio of HT and wing lift curve slopes
p_{ht}	[-]	Substituted variable = $1 + 2 \cdot \text{taper}$
q_{ht}	[-]	Substituted variable = $1 + \text{taper}$
w_{fuse}	[m]	Fuselage width
x_w	[m]	Position of wing aerodynamic center
x_{CG}	[m]	x-location of CG
$y\bar{c}_{ht}$	[m]	Spanwise location of mean aerodynamic chord

Table 8: Fixed variables in the horizontal tail model

Constants	Units	Description
$C_{L_{ht,max}}$	[-]	Max horizontal tail lift coefficient
$C_{L_{w,max}}$	[-]	Max lift coefficient, wing
$C_{m_{ac}}$	[-]	Moment coefficient about aerodynamic centre (wing)
$S.M._{min}$	[-]	Minimum allowed stability margin
V_{ne}	[$\frac{m}{s}$]	Never exceed velocity
Δx_{CG}	[m]	CG travel range
$\alpha_{ht,max}$	[-]	Max angle of attack, htail
η_{ht}	[-]	Tail efficiency
$\lambda_{ht,min}$	[-]	Minimum horizontal tail taper ratio
ρ_0	[$\frac{kg}{m^3}$]	Air density (0 ft)
$\tan(\Lambda_{ht})$	[-]	tangent of horizontal tail sweep
g	[$\frac{m}{s^2}$]	Gravitational acceleration

1. Horizontal Tail Geometry and Structure

The horizontal tail model employs many of the same geometric constraints as the wing and vertical tail. More specifically, analogous versions of Constraints (51) to (55) and Constraints (107)

to (109) enforce planform relationships and constrain the horizontal tail moment arm, respectively. As with the vertical tail, Constraint (52) needs to be implemented as a signomial equality constraint. The horizontal tail also reuses the same structural model from [1].

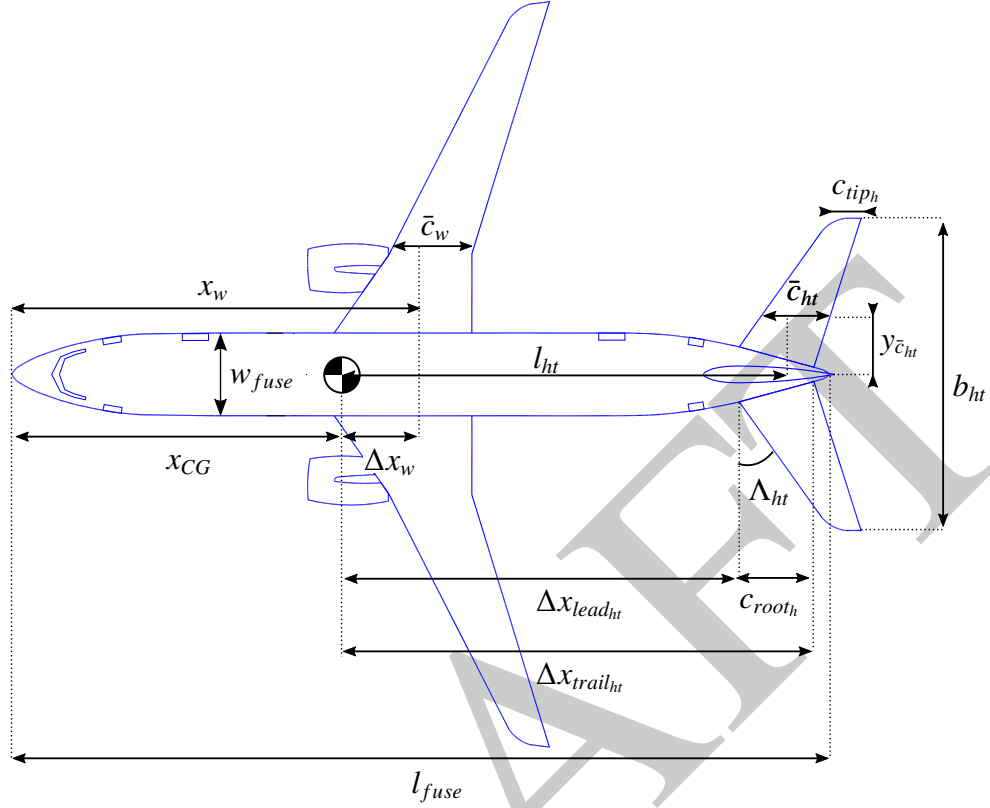


Figure 5: Geometric variables of the horizontal tail model (adapted from [21])

2. Trim Condition

The first sizing requirement is that the aircraft must satisfy the trim condition [29], which implicitly requires that the full aircraft moment coefficient be zero.

$$\frac{x_w}{\bar{c}_w} \leq \frac{x_{CG}}{\bar{c}_w} + \frac{C_{mac}}{C_{L_w}} + \frac{V_{ht} C_{L_{ht}}}{C_{L_w}} \quad (119)$$

Thin airfoil theory is used to constrain the horizontal tail's isolated lift curve slope [30].

$$C_{L_{ht}} = C_{L_{\alpha,ht}} \alpha \quad (120)$$

However, the horizontal tail's lift curve slope is reduced by downwash, ϵ , from the wing and fuselage [22]. Note $\eta_{h_{lift}}$ is the horizontal tail sectional lift efficiency.

$$C_{L_{\alpha,ht}} = C_{L_{\alpha,ht0}} \left(1 - \frac{\partial \epsilon}{\partial \alpha} \right) \eta_{h_{lift}} \quad (121)$$

The downwash can be approximated as the downwash far behind an elliptically loaded wing.

$$\epsilon \approx \frac{2C_{L_w}}{\pi AR_w} \quad (122)$$

$$\Rightarrow \frac{\partial \epsilon}{\partial \alpha} \approx \frac{2C_{L_{\alpha,w}}}{\pi AR_w} \quad (123)$$

Thus, an additional posynomial constraint is introduced to constrain the corrected lift curve slope.

$$C_{L_{\alpha,ht}} + \frac{2C_{L_{\alpha,w}}}{\pi AR_w} \eta_{ht} C_{L_{\alpha,ht0}} \leq C_{L_{\alpha,ht0}} \eta_{ht} \quad (124)$$

3. Minimum Stability Margin

The second condition is that the aircraft must maintain a minimum stability margin at both the forward and aft CG limits [29].

$$S.M._{min} + \frac{\Delta x_{CG}}{\bar{c}_w} + \frac{C_{m_{ac}}}{C_{L_{w,max}}} \leq V_{ht} m_{ratio} + \frac{V_{ht} C_{L_{h,max}}}{C_{L_{w,max}}} \quad (125)$$

The ratio of the horizontal tail and wing lift curve slopes, m_{ratio} , appears in Equation (125) and is constrained using the relationship in [29]. The constraint is a signomial equality because it is not possible to know a priori whether there will be upward or downward pressure on m_{ratio} .

$$m_{ratio} = \left(1 + \frac{2}{AR_w}\right) \left(1 + \frac{2}{AR_{ht}}\right) \quad (126)$$

4. Stability Margin

The third condition is that the stability margin must be greater than a minimum specified value for all intermediate CG locations.

$$S.M. \leq \frac{x_w - x_{CG}}{\bar{c}_w} \quad (127)$$

$$S.M. \geq S.M._{min} \quad (128)$$

5. Horizontal Tail Drag

The horizontal tail employs the same drag model as the wing (Constraints (93) to (97)), with the exception of the parasitic drag coefficient fit. The wing's parasitic drag fit (95) is replaced by a fit to XFOIL [24] data for the TASOPT [5] T-series airfoils. The TASOPT T-series airfoils are horizontal tail airfoils intended for transonic use. The fit considers airfoil thickness, Reynolds number, and Mach number. The softmax affine function fit is developed with GPfit [10, 25] and has an RMS error of 1.14%.

$$\begin{aligned} C_{D0_{ht}}^{6.49} &\geq 5.288 \times 10^{-20} (Re_h)^{0.901} (\tau_h)^{0.912} (M)^{8.645} \\ &\quad + 1.676 \times 10^{-28} (Re_h)^{0.351} (\tau_h)^{6.292} (M)^{10.256} \\ &\quad + 7.098 \times 10^{-25} (Re_h)^{1.395} (\tau_h)^{1.962} (M)^{0.567} \end{aligned} \quad (129)$$

$$\begin{aligned}
& + 3.731 \times 10^{-14} (Re_h)^{-2.574} (\tau_h)^{3.128} (M)^{0.448} \\
& + 1.443 \times 10^{-12} (Re_h)^{-3.910} (\tau_h)^{4.663} (M)^{7.689}
\end{aligned}$$

VI. Fuselage Model

At a high level, the purpose of a conventional commercial aircraft fuselage can be decomposed into two primary functions: integrating and connecting all of the subsystems (e.g. wing, tail, landing gear), and carrying the payload, which typically consists of passengers, luggage, and sometimes cargo. The design of the fuselage is therefore coupled with virtually every aircraft subsystem.

Drela [5] performs a detailed, but still approximate, analysis of fuselage structure and weight, considering pressure loads, torsion loads, bending loads, buoyancy weight, window weight, payload-proportional weights, the floor, and the tail cone. The majority of the constraints in this model are adapted directly from these equations.

A. Model Assumptions

This model assumes a single circular-cross-section fuselage. This is an approximation, since narrow-body aircraft like the Boeing 737 and Airbus A320 do not have perfectly circular cross sections.

The floor structural model and the horizontal bending model assume uniform floor loading. The model leverages the analytical bending models from Drela [5], which makes assumptions about symmetry in bending loads. Shell buckling is not explicitly modeled while designing bending structure, but is accounted for by the implementation of a lower yield stress for bending reinforcement material relative to the nominal yield stress of the material.

B. Model Description

The fuselage model has 84 free variables and 96 constraints.

Table 9: Free variables in the fuselage model

Free Variables	Units	Description
A_{0h}	m^2	Horizontal bending area constant A_{0h}
$A_{1h_{Land}}$	m	Horizontal bending area constant A_{1h} (landing case)
$A_{1h_{MLF}}$	m	Horizontal bending area constant A_{1h} (max aero load case)
$A_{2h_{Land}}$	$[-]$	Horizontal bending area constant A_{2h} (landing case)
$A_{2h_{MLF}}$	$[-]$	Horizontal bending area constant A_{2h} (max aero load case)
A_{floor}	m^2	Floor beam x-sectional area
A_{fuse}	m^2	Fuselage x-sectional area
$A_{hbendb_{Land}}$	m^2	Horizontal bending area at rear wingbox (landing case)
$A_{hbendb_{MLF}}$	m^2	Horizontal bending area at rear wingbox (max aero load case)
$A_{hbendf_{Land}}$	m^2	Horizontal bending area at front wingbox (landing case)
$A_{hbendf_{MLF}}$	m^2	Horizontal bending area at front wingbox (max aero load case)
A_{skin}	m^2	Skin cross sectional area
A_{vbendb}	m^2	Vertical bending material area at rear wingbox
B_{0v}	m^2	Vertical bending area constant B_0
B_{1v}	m	Vertical bending area constant B_1
$C_{D_{fuse}}$	$[-]$	Fuselage drag coefficient

D_{fuse}	N	Fuselage drag
$I_{h_{shell}}$	m^4	Shell horizontal bending inertia
$I_{v_{shell}}$	m^4	Shell vertical bending inertia
$L_{ht_{max}}$	N	Horizontal tail maximum load
$L_{vt_{max}}$	N	Vertical tail maximum load
M	[-]	Cruise Mach number
M_{floor}	$N \cdot m$	Max bending moment in floor beams
P_{floor}	N	Distributed floor load
R_{fuse}	m	Fuselage radius
S_{bulk}	m^2	Bulkhead surface area
S_{floor}	N	Maximum shear in floor beams
S_{nose}	m^2	Nose surface area
V_{∞}	$[\frac{m}{s}]$	Cruise velocity
V_{bulk}	m^3	Bulkhead skin volume
V_{cabin}	m^3	Cabin volume
V_{cone}	m^3	Cone skin volume
V_{cyl}	m^3	Cylinder skin volume
V_{floor}	m^3	Floor volume
V_{hbend_b}	m^3	Horizontal bending material volume b
V_{hbend_c}	m^3	Horizontal bending material volume c
V_{hbend_f}	m^3	Horizontal bending material volume f
V_{hbend}	m^3	Horizontal bending material volume
V_{nose}	m^3	Nose skin volume
V_{vbend_b}	m^3	Vertical bending material volume b
V_{vbend_c}	m^3	Vertical bending material volume c
V_{vbend}	m^3	Vertical bending material volume
W_{apu}	lbf	APU weight
W_{buoy}	lbf	Buoyancy weight
W_{cone}	lbf	Cone weight
W_{fix}	lbf	Fixed weights (pilots, cockpit seats, navcom)
W_{floor}	lbf	Floor weight
W_{fuse}	lbf	Fuselage weight
W_{hbend}	lbf	Horizontal bending material weight
W_{insul}	lbf	Insulation material weight
W_{lugg}	lbf	Passenger luggage weight
W_{padd}	lbf	Misc weights (galley, toilets, doors etc.)
W_{pass}	lbf	Passenger weight
$W_{payload}$	lbf	Payload weight
W_{seat}	lbf	Seating weight
W_{shell}	lbf	Shell weight
W_{skin}	lbf	Skin weight
W_{tail}	lbf	Total tail weight
W_{vbend}	lbf	Vertical bending material weight
W_{window}	lbf	Window weight
λ_{cone}	[-]	Tailcone radius taper ratio
ρ_{∞}	$[\frac{kg}{m^3}]$	Freestream density
ρ_{cabin}	$[\frac{kg}{m^3}]$	Cabin air density
σ_x	$[\frac{N}{m^2}]$	Axial stress in skin
σ_{M_h}	$[\frac{N}{m^2}]$	Horizontal bending material stress
σ_{M_v}	$[\frac{N}{m^2}]$	Vertical bending material stress

σ_{θ}	$\frac{N}{m^2}$	Skin hoop stress
τ_{cone}	$\frac{N}{m^2}$	Shear stress in tail cone
c_0	m	Root chord of the wing
h_{fuse}	m	Fuselage height
l_{cone}	m	Cone length
l_{floor}	m	Floor length
l_{fuse}	m	Fuselage length
l_{shell}	m	Shell length
n_{rows}	[-]	Number of rows
n_{seat}	[-]	Number of seats
t_{shell}	m	Shell thickness
t_{skin}	m	Skin thickness
w_{aisle}	m	Aisle width
w_{floor}	m	Floor half-width
w_{fuse}	m	Fuselage half-width
x_b	m	x-location of back of wingbox
x_f	m	x-location of front of wingbox
$x_{hbend_{Land}}$	ft	Horizontal zero bending location (landing case)
$x_{hbend_{MLF}}$	ft	Horizontal zero bending location (maximum aero load case)
x_{shell1}	m	Start of cylinder section
x_{shell2}	m	End of cylinder section
x_{tail}	m	x-location of tail
x_{vbend}	ft	Vertical zero bending location
x_{wing}	m	x-location of wing c/4

Table 10: Fixed variables in the fuselage model

Constants	Units	Description
M_{fuseD}	[-]	Fuselage drag reference Mach number
N_{land}	[-]	Emergency landing load factor
N_{lift}	[-]	Wing maximum load factor
P_{cabin}	$\frac{N}{m^2}$	Cabin air pressure
R	$\frac{J}{kgK}$	Air specific heat
S_{PR}	[-]	Number of seats per row
T_{cabin}	[K]	Cabin air temperature
W''_{floor}	$\frac{N}{m^2}$	Floor weight/area density
W''_{insul}	$\frac{N}{m^2}$	Weight/area density of insulation material
W'_{seat}	N	Weight per seat
W'_{window}	$\frac{N}{m}$	Weight/length density of windows
$W_{avg,pass,total}$	lbf	Average passenger weight including payload
$W_{avg,pass}$	lbf	Average passenger weight
W_{cargo}	lbf	Cargo weight
$W_{carryon}$	lbf	Ave. carry-on weight
$W_{checked}$	lbf	Ave. checked bag weight
W_{fix}	lbf	Fixed weights (pilots, cockpit seats, navcom)
ΔP_{over}	psi	Cabin overpressure
ΔR_{fuse}	m	Fuselage extension height
λ_{cone}	[-]	Tailcone radius taper ratio
ρ_{bend}	$\frac{kg}{m^3}$	Stringer density
ρ_{cargo}	$\frac{kg}{m^3}$	Cargo density
ρ_{cone}	$\frac{kg}{m^3}$	Cone material density
ρ_{floor}	$\frac{kg}{m^3}$	Floor material density

ρ_{lugg}	$\frac{\text{kg}}{\text{m}^3}$	Luggage density
ρ_{skin}	$\frac{\text{kg}}{\text{m}^3}$	Skin density
σ_{bend}	$\frac{\text{N}}{\text{m}^2}$	Bending material stress
σ_{floor}	$\frac{\text{N}}{\text{m}^2}$	Max allowable floor stress
σ_{skin}	$\frac{\text{N}}{\text{m}^2}$	Max allowable skin stress
τ_{floor}	$\frac{\text{N}}{\text{m}^2}$	Max allowable shear web stress
f_{apu}	[-]	APU weight as fraction of payload weight
f_{fadd}	[-]	Fractional added weight of local reinforcements
f_{frame}	[-]	Fractional frame weight
$f_{lugg,1}$	[-]	Proportion of passengers with one suitcase
$f_{lugg,2}$	[-]	Proportion of passengers with two suitcases
f_{padd}	[-]	Other misc weight as fraction of payload weight
f_{seat}	[-]	Fractional seat weight
f_{string}	[-]	Fractional stringer weight
g	$\frac{\text{m}}{\text{s}^2}$	Acceleration due to gravity
h_{floor}	m	Floor beam height
l_{nose}	m	Nose length
n_{pass}	[-]	Number of passengers
p_s	cm	Seat pitch
p_{λ_v}	[-]	$1 + 2 \times \text{Tail taper ratio}$
r_E	[-]	Ratio of stringer/skin moduli
r_{M_h}	[-]	Horizontal inertial relief factor
r_{M_v}	[-]	Vertical inertial relief factor
$r_{w/c}$	[-]	Wingbox width-to-chord ratio
w_{aisle}	m	Aisle width
w_{seat}	m	Seat width
w_{sys}	m	Width between cabin and skin for systems

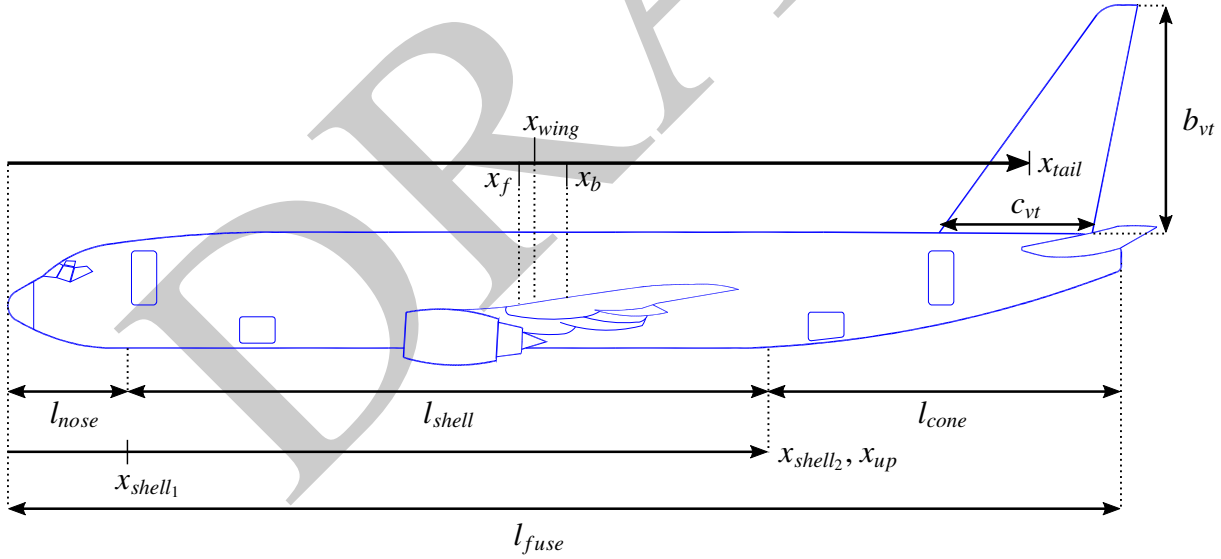


Figure 6: Geometric variables of the fuselage model (adapted from [21])

1. Cross-sectional geometry constraints

The fuselage must be wide enough to accommodate the width of the seats in a row and the width of the aisle.

$$2w_{fuse} \geq (SPR)w_{seat} + w_{aisle} + 2w_{sys} \quad (130)$$

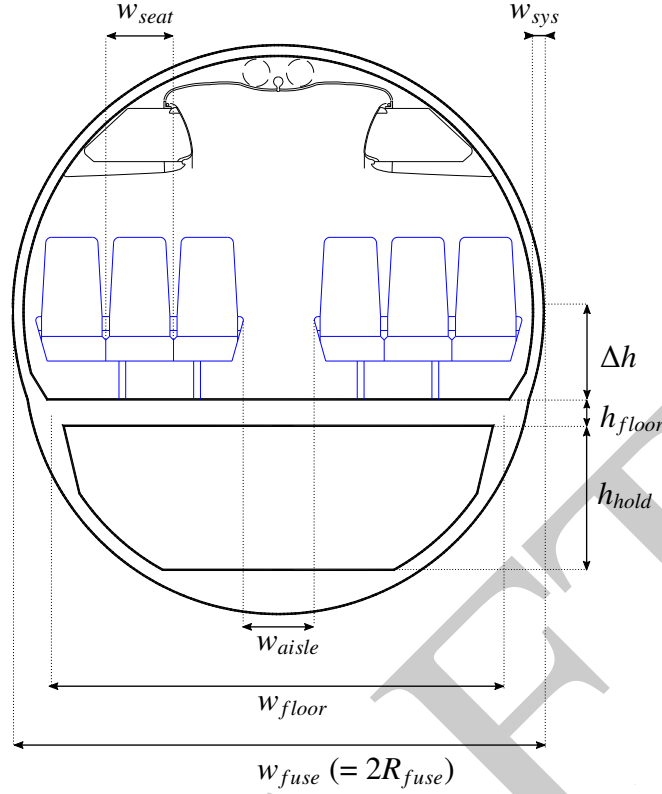


Figure 7: Geometric variables (cross-section) of the fuselage model (adapted from [21])

The cross sectional area of the fuselage skin is lower bounded using a thin walled cylinder assumption.

$$A_{skin} \geq 2\pi R_{fuse} t_{skin} \quad (131)$$

The cross sectional area of the fuselage is lower bounded using the radius of the fuselage.

$$A_{fuse} \geq \pi R_{fuse}^2 \quad (132)$$

2. Pressure loading constraints

The axial and hoop stresses in the fuselage skin are constrained by the pressurization load due to the difference between cabin pressure and ambient pressure at cruise altitude. The thickness of the skin is therefore sized by the maximum allowable stress of the chosen material.

$$\sigma_x = \frac{\Delta P_{over}}{2} \frac{R_{fuse}}{t_{shell}} \quad (133)$$

$$\sigma_\theta = \Delta P_{over} \frac{R_{fuse}}{t_{skin}} \quad (134)$$

$$\sigma_{skin} \geq \sigma_x \quad (135)$$

$$\sigma_{skin} \geq \sigma_\theta \quad (136)$$

3. Floor loading constraints

The floor must be designed to withstand at least the weight of the payload and seats multiplied by a safety factor for an emergency landing.

$$P_{floor} \geq N_{land}(W_{payload} + W_{seat}) \quad (137)$$

The maximum moment and shear in the floor are determined based on this design load and the width of the floor, assuming that the floor/wall joints are pinned and there are no center supports.

$$S_{floor} = \frac{P_{floor}}{2} \quad (138)$$

$$M_{floor} = \frac{P_{floor}W_{floor}}{8} \quad (139)$$

The floor beam cross sectional area is constrained by the maximum allowable cap stress and shear web stress for the beams.

$$A_{floor} \geq 1.5 \frac{S_{floor}}{\tau_{floor}} + 2 \frac{M_{floor}}{\sigma_{floor}h_{floor}} \quad (140)$$

4. 3-dimensional geometry constraints

The nose must be long enough to have an aerodynamic profile and to accommodate the cockpit. A reasonable, but arbitrary, lower bound is employed for this work [5].

$$l_{nose} \geq 5.2 \text{ m} \quad (141)$$

The cylindrical shell of the fuselage sits between the nosecone and tailcone. The variables x_{shell1} and x_{shell2} define the beginning and end of the cylindrical section of the fuselage, respectively, in the aircraft x-axis.

$$x_{shell1} = l_{nose} \quad (142)$$

$$x_{shell2} \geq l_{nose} + l_{shell} \quad (143)$$

The number of seats is equal to the product of the seats per row and the number of rows. Note that non-integer numbers of rows are allowed and necessary for GP compatibility. It is assumed that the load factor is one, so that the number of passengers is equal to the number of seats.

$$n_{seat} = (SPR)n_{rows} \quad (144)$$

$$n_{pass} = n_{seat} \quad (145)$$

The seat pitch and the number of rows of seats constrain the length of the shell. The passenger floor length is lower bounded by the shell length and twice the fuselage radius, to account for the space provided by pressure bulkheads.

$$l_{shell} \geq n_{rows}p_s \quad (146)$$

$$l_{floor} \geq 2R_{fuse} + l_{shell} \quad (147)$$

The length of the fuselage is constrained by the sum of the nose, shell and tail cone lengths. A signomial equality is needed, because increased l_{fuse} is not coupled directly to increased structural weight although it results in improved tail control authority.

$$l_{fuse} = l_{nose} + l_{shell} + l_{cone} \quad (148)$$

Other locations to constrain are the wing mid-chord and the wingbox fore and aft bulkheads, which serve as integration limits when calculating bending loads.

$$x_f \leq x_{wing} + 0.5c_0r_{w/c} \quad (149)$$

$$x_b + 0.5c_0r_{w/c} \geq x_{wing} \quad (150)$$

The skin surface area, and, in turn, skin volume for the nose, main cabin, and rear bulkhead are constrained. The surface area of the nose, which is approximated as an ellipse, is lower bounded using Cantrell's approximation [5].

$$S_{nose}^{\frac{8}{5}} \geq \left(2\pi R_{fuse}^2\right)^{\frac{8}{5}} \left(\frac{1}{3} + \frac{2}{3} \left(\frac{l_{nose}}{R_{fuse}}\right)^{\frac{8}{5}}\right) \quad (151)$$

$$S_{bulk} = 2\pi R_{fuse}^2 \quad (152)$$

$$V_{cyl} = A_{skin}l_{shell} \quad (153)$$

$$V_{nose} = S_{nose}t_{skin} \quad (154)$$

$$V_{bulk} = S_{bulk}t_{skin} \quad (155)$$

The cabin volume is constrained assuming a cylinder with hemispherical end caps. This is necessary for capturing buoyancy weight.

$$V_{cabin} \geq A_{fuse} \left(\frac{2}{3}l_{nose} + l_{shell} + \frac{2}{3}R_{fuse}\right) \quad (156)$$

5. Tail cone constraints

The tail cone needs to be able to transfer the loads exerted on the vertical tail to the rest of the fuselage. The maximum torsion moment imparted by the vertical tail depends on the maximum force exerted on the tail as well as its span and taper ratio. This torsion moment, along with the cone cross sectional area and the maximum shear stress of the cone material, bounds the necessary cone skin thickness. The cone cross sectional area, which varies along the cone, is coarsely approximated to be the fuselage cross sectional area (i.e. the cross sectional area of the cone base).

$$Q_v = \frac{L_{vt_{max}}b_{vt}}{3} \frac{1 + 2\lambda_v}{1 + \lambda_v} \quad (157)$$

$$t_{cone} = \frac{Q_v}{2A_{fuse}\tau_{cone}} \quad (158)$$

The volume of the cone is a definite integral from the base to the tip of the cone. This integral is evaluated [5] and combined with Equations (157) and (158) to give a single signomial constraint

on the cone skin volume.

$$R_{fuse}\tau_{cone}(1 + p_{\lambda_v})V_{cone}\frac{1 + \lambda_{cone}}{4l_{cone}} \geq L_{vt_{max}}b_{vt}\frac{p_{\lambda_v}}{3} \quad (159)$$

A change of variables is used for compatibility with the tail model, which uses $p_{\lambda_v} = 1 + 2\lambda_v$ to make a structural constraint GP-compatible. The same taper lower bound is introduced as in the tail model.

$$p_{\lambda_v} \geq 1.6 \quad (160)$$

The cone skin shear stress is constrained to equal the maximum allowable stress in the skin material.

$$\tau_{cone} = \sigma_{skin} \quad (161)$$

The tail cone taper ratio constrains the length of the cone relative to the radius of the fuselage.

$$l_{cone} = \frac{R_{fuse}}{\lambda_{cone}} \quad (162)$$

6. Fuselage area moment of inertia constraints

The fuselage shell consists of the skin and stringers. Its area moment of inertia determines how effectively the fuselage is able to resist bending loads. A shell with uniform skin thickness and stringer density has a constant area moment of inertia in both of its bending axes, shown by the dark red line in the lower plot of Figure 8.

To be consistent with [5], the horizontal bending moments are defined as the moments around the aircraft's y-axis, caused by horizontal tail loads and fuselage inertial loads, and vertical bending moments as the moments around the aircraft's z-axis, caused by vertical tail loads.

The effective modulus-weight shell thickness is lower bounded by assuming that only the skin and stringers contribute to bending. This constraint also uses an assumed fractional weight of stringers that scales with the thickness of the skin.

$$t_{shell} \geq t_{skin} \left(1 + f_{string} r_E \frac{\rho_{skin}}{\rho_{bend}} \right) \quad (163)$$

It is important to consider the effects of pressurization on the yield strength of the bending material. Since pressurization stresses the airframe, the actual yield strength of the fuselage bending material is lower than its nominal yield strength, an effect captured using posynomial constraints.

$$\sigma_{M_h} + r_E \frac{\Delta P_{over} R_{fuse}}{2t_{shell}} \leq \sigma_{bend} \quad (164)$$

$$\sigma_{M_v} + r_E \frac{\Delta P_{over} R_{fuse}}{2t_{shell}} \leq \sigma_{bend} \quad (165)$$

The aircraft shell, which is composed of the pressurized skin and stringers, must satisfy the following horizontal and vertical area moment of inertia constraints.

$$I_{hshell} \leq \pi R_{fuse}^3 t_{shell} \quad (166)$$

$$I_{vshell} \leq \pi R_{fuse}^3 t_{shell} \quad (167)$$

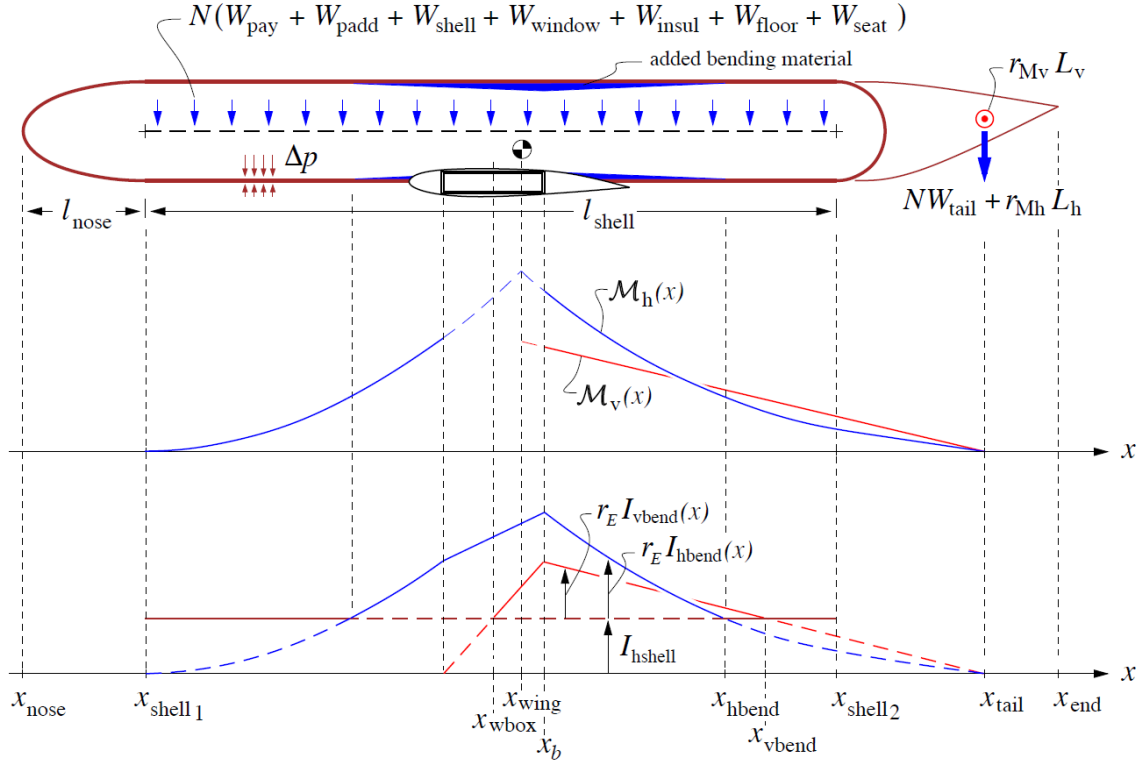


Figure 8: TASOPT fuselage bending models (from [5]). The top graph shows the bending load distribution on the fuselage, whereas the bottom graph shows the area moment of inertia distribution. The horizontal bending loads are shown in blue, and the vertical bending loads are shown in red.

7. Horizontal bending model

There are two load cases that determine the required Horizontal Bending Material (HBM): maximum load factor (MLF) at V_{ne} , where

$$N = N_{lift} \quad (168)$$

$$L_{ht} = L_{ht_{max}} \quad (169)$$

and emergency landing impact, where

$$N = N_{land} \quad (170)$$

$$L_{ht} = 0. \quad (171)$$

Both load cases are considered at the aircraft's maximum takeoff weight (MTOW). The constraints for each case are distinguished by the subscripts *MLF* and *Land*. Assuming the fuselage weight is uniformly distributed throughout the shell, the bending loads due to fuselage inertial loads increase quadratically from the ends of the fuselage shell to the aircraft CG, as shown by the blue line representing $M_h(x)$ in Figure 8. The tail loads are point loads at x_{tail} , and so the horizontal tail moment increases linearly from x_{tail} to the aircraft's CG. In the maximum load factor case, the maximum moment exerted by the horizontal tail is superimposed on the maximum fuselage inertial moment at load factor N_{lift} to size the HBM required. For the emergency landing impact

case, only the fuselage inertial loads are considered at N_{land} , assuming an unloaded horizontal tail.

Several intermediate variables are introduced and used in constraints that capture HBM relationships. A_{0h} represents the HBM area that is contributed by the aircraft shell.

$$A_{0h} = \frac{I_{hshell}}{r_E h_{fuse}^2} \quad (172)$$

Variables $A_{1h_{Land}}$ and $A_{1h_{MLF}}$ are the HBM lengths that are required to sustain bending loads from the tail. Note that as the distance from the tail increases, the moment exerted from the tail increases linearly.

$$A_{1h_{Land}} \geq N_{land} \frac{W_{tail} + W_{apu}}{h_{fuse} \sigma_{M_h}} \quad (173)$$

$$A_{1h_{MLF}} \geq N_{lift} \frac{W_{tail} + W_{apu} + r_{M_h} L_{ht_{max}}}{h_{fuse} \sigma_{M_h}} \quad (174)$$

Variables $A_{2h_{Land}}$ and $A_{2h_{MLF}}$ represent the HBM required to sustain the distributed loads in the fuselage. As the distance from the nose or the tail increases, the moment exerted due to the distributed load grows with the square of length.

$$A_{2h_{Land}} \geq N_{land} \frac{W_{payload} + W_{padd} + W_{shell} + W_{window} + W_{insul} + W_{floor} + W_{seat}}{2l_{shell} h_{fuse} \sigma_{bend}} \quad (175)$$

$$A_{2h_{MLF}} \geq N_{lift} \frac{W_{payload} + W_{padd} + W_{shell} + W_{window} + W_{insul} + W_{floor} + W_{seat}}{2l_{shell} h_{fuse} \sigma_{M_h}} \quad (176)$$

Bending reinforcement material in the aircraft exists where the shell inertia is insufficient to sustain the local bending moment. Constraints are used to determine the location over the rear fuselage x_{hbend_ζ} forward of which additional HBM is required. Some simple constraints on geometry are added to ensure a meaningful solution. Constraints (177) through (184) occur for both aforementioned load cases in the model (with subscript ζ replaced by MLF or $Land$) for worst-case fuselage sizing, but have been included once in the paper to reduce redundancy.

$$A_{0h} = A_{2h_\zeta} (x_{shell2} - x_{hbend_\zeta})^2 + A_{1h_\zeta} (x_{tail} - x_{hbend_\zeta}) \quad (177)$$

$$x_{hbend_\zeta} \geq x_{wing} \quad (178)$$

$$x_{hbend_\zeta} \leq l_{fuse} \quad (179)$$

To be able to constrain the volume of HBM required, the area of HBM required must be constrained and integrated over the length of the fuselage. As shown by [5], with some conservative approximation, the volume of HBM may be determined through the integration of the forward and rear wingbox HBM areas over the rear fuselage.

$$A_{hbendf_\zeta} \geq A_{2h_\zeta} (x_{shell2} - x_f)^2 + A_{1h_\zeta} (x_{tail} - x_f) - A_{0h} \quad (180)$$

$$A_{hbendb_\zeta} \geq A_{2h_\zeta} (x_{shell2} - x_b)^2 + A_{1h_\zeta} (x_{tail} - x_b) - A_{0h} \quad (181)$$

HBM volumes forward, over and behind the wingbox are lower bounded by the integration of

the HBM areas over the three fuselage sections.

$$V_{hbend_f} \geq \frac{A_{2h_\zeta}}{3}((x_{shell2} - x_f)^3 - (x_{shell2} - x_{hbend_\zeta})^3) \quad (182)$$

$$+ \frac{A_{1h_\zeta}}{2}((x_{tail} - x_f)^2 - (x_{tail} - x_{hbend_\zeta})^2) - A_{0h}(x_{hbend_\zeta} - x_f)$$

$$V_{hbend_b} \geq \frac{A_{2h_\zeta}}{3}((x_{shell2} - x_b)^3 - (x_{shell2} - x_{hbend_\zeta})^3) \quad (183)$$

$$+ \frac{A_{1h_\zeta}}{2}((x_{tail} - x_b)^2 - (x_{tail} - x_{hbend_\zeta})^2) - A_{0h}(x_{hbend_\zeta} - x_b)$$

$$V_{hbend_c} \geq 0.5(A_{hbendf_\zeta} + A_{hbendb_\zeta})c_0r_{w/c} \quad (184)$$

The total HBM volume is lower bounded by the sum of the volumes of HBM required in each fuselage section.

$$V_{hbend} \geq V_{hbend_c} + V_{hbend_f} + V_{hbend_b} \quad (185)$$

8. Vertical bending model

The Vertical Bending Material (VBM) is constrained by considering the maximum tail loads that a fuselage must sustain. The vertical bending moment, shown in red as $M_v(x)$ in Figure 8, increases linearly from the tail to the aircraft CG, since the tail lift is assumed to be a point force.

As with horizontal bending, several intermediate variables are introduced and used in constraints that capture VBM relationships. B_{1v} is the VBM length required to sustain the maximum vertical tail load $L_{vt_{max}}$. When multiplied by the moment arm of the tail relative to the fuselage cross-sectional location, it gives the local VBM area required to sustain the loads.

$$B_{1v} = \frac{r_{M_v} L_{vt_{max}}}{w_{fuse} \sigma_{M_v}} \quad (186)$$

B_{0v} is the equivalent VBM area provided by the fuselage shell.

$$B_{0v} = \frac{I_{vshell}}{r_E w_{fuse}^2} \quad (187)$$

Since tail loads are the only vertical loads to consider, the location forward of which additional bending material is required can be determined. x_{vbend} is the location where the vertical bending moment of the inertia of the fuselage is exactly enough to sustain the maximum vertical bending loads from the tail, expressed by a signomial equality.

$$B_{0v} = B_{1v}(x_{tail} - x_{vbend}) \quad (188)$$

$$x_{vbend} \geq x_{wing} \quad (189)$$

$$x_{vbend} \leq l_{fuse} \quad (190)$$

The VBM area required at the rear of the wingbox is lower bounded by the tail bending moment area minus the shell vertical bending moment area.

$$A_{vbend_b} \geq B_{1v}(x_{tail} - x_b) - B_{0v} \quad (191)$$

The vertical bending volume rear of the wingbox is then constrained by integrating A_{vbend} over the rear fuselage, which yields the following constraint.

$$V_{vbend_b} \geq 0.5B_{1v}((x_{tail} - x_b)^2 - (x_{tail} - x_{vbend})^2) - B_{0v}(x_{vbend} - x_b) \quad (192)$$

The vertical bending volume over the wingbox is the average of the bending area required in the front and back of the wingbox. Since no vertical bending reinforcement is required in the forward fuselage, the resulting constraint is simply:

$$V_{vbend_c} \geq 0.5A_{vbend_b}c_0r_{w/c} \quad (193)$$

The total vertical bending reinforcement volume is the sum of the volumes over the wingbox and the rear fuselage.

$$V_{vbend} \geq V_{vbend_b} + V_{vbend_c} \quad (194)$$

9. Weight build-up constraints

The weight of the fuselage skin is the product of the skin volumes (bulkhead, cylindrical shell, and nosecone) and the skin density.

$$W_{skin} \geq \rho_{skin}g(V_{bulk} + V_{cyl} + V_{nose}) \quad (195)$$

The weight of the fuselage shell is then constrained by accounting for the weights of the frame, stringers, and other structural components, all of which are assumed to scale with the weight of the skin.

$$W_{shell} \geq W_{skin}(1 + f_{fadd} + f_{frame} + f_{string}) \quad (196)$$

The weight of the floor is lower bounded by the density of the floor beams multiplied by the floor beam volume, in addition to an assumed weight/area density for planking.

$$V_{floor} \geq A_{floor}w_{floor} \quad (197)$$

$$W_{floor} \geq V_{floor}\rho_{floor}g + W''_{floor}l_{floor}w_{floor} \quad (198)$$

As with the shell, the tail cone weight is bounded using assumed proportional weights for additional structural elements, stringers, and frames.

$$W_{cone} \geq \rho_{cone}gV_{cone}(1 + f_{fadd} + f_{frame} + f_{string}) \quad (199)$$

The weight of the horizontal and vertical bending material is the product of the bending material density and the HBM and VBM volumes required respectively.

$$W_{hbend} \geq \rho_{bend}gV_{hbend} \quad (200)$$

$$W_{vbend} \geq \rho_{bend}gV_{vbend} \quad (201)$$

The weight of luggage is lower bounded by a buildup of 2-checked-bag customers, 1-checked-bag customers, and average carry-on weight.

$$W_{lugg} \geq 2W_{checked}f_{lugg,2}n_{pass} + W_{checked}f_{lugg,1}n_{pass} + W_{carryon} \quad (202)$$

The window and insulation weight are lower bounded using assumed weight/length and weight/area densities respectively. It is assumed that only the passenger compartment of the the cabin is insulated and that the passenger compartment cross sectional area is approximately 55% of the fuselage cross sectional area.

$$W_{window} = W'_{window} l_{shell} \quad (203)$$

$$W_{insul} \geq W''_{insul} (0.55 (S_{bulk} + S_{nose}) + 1.1\pi R_{fuse} l_{shell}) \quad (204)$$

The APU and other payload proportional weights are accounted for using weight fractions. W_{padd} includes flight attendants, food, galleys, toilets, furnishing, doors, lighting, air conditioning, and in-flight entertainment systems. The total seat weight is a product of the weight per seat and the number of seats.

$$W_{apu} = W_{payload} f_{apu} \quad (205)$$

$$W_{padd} = W_{payload} f_{padd} \quad (206)$$

$$W_{seat} = W'_{seat} n_{seat} \quad (207)$$

The effective buoyancy weight of the aircraft is constrained using a specified cabin pressure p_{cabin} , the ideal gas law and the approximated cabin volume. A conservative approximation for the buoyancy weight that does not subtract the ambient air density from the cabin air density is used.

$$\rho_{cabin} = \frac{p_{cabin}}{RT_{cabin}} \quad (208)$$

$$W_{buoy} = \rho_{cabin} g V_{cabin} \quad (209)$$

There are two methods in the model that can be used to lower bound the payload weight. The first is the sum of the cargo, luggage, and passenger weights (Constraint (211)). The second is through the definition of variable $W_{avg.pass_{total}}$, which is an average payload weight per passenger metric (Constraint (212)). For the purposes of this paper, the second method is used, and as a result Constraint (211) is inactive.

$$W_{pass} = W_{avg.pass} n_{pass} \quad (210)$$

$$W_{payload} \geq W_{cargo} + W_{lugg} + W_{pass} \quad (211)$$

$$W_{payload} \geq W_{avg.pass_{total}} n_{pass} \quad (212)$$

The total weight of the fuselage is lower bounded by the sum of all of the constituent weights. The fixed weight W_{fix} incorporates pilots, cockpit windows, cockpit seats, flight instrumentation, navigation and communication equipment, which are expected to be roughly the same for all aircraft [5].

$$W_{fuse} \geq W_{apu} + W_{buoy} + W_{cone} + W_{floor} + W_{hbend} + W_{vbend} + W_{insul} + W_{padd} + W_{seat} + W_{shell} + W_{window} + W_{fix} \quad (213)$$

10. Aerodynamic constraints

The drag of the fuselage is constrained using $C_{D_{fuse}}$ from TASOPT, which calculates the drag using a pseudo-axisymmetric viscous/inviscid calculation, and scaling appropriately by fuselage

dimensions and Mach number.

$$D_{fuse} = \frac{1}{2} \rho_{\infty} V_{\infty}^2 C_{D_{fuse}} \left(l_{fuse} R_{fuse} \frac{M^2}{M_{fuseD}^2} \right) \quad (214)$$

VII. Landing Gear Model

The purpose of the landing gear is to support the weight of the aircraft and allow it to manoeuvre while it is on the ground, including during taxi, takeoff, and landing. Including the landing gear in aircraft MDO is important, not only because it typically weighs between three and six percent of the maximum aircraft takeoff weight [31], but also because of how coupled its design is to other subsystems, particularly the fuselage, wings, and engines. The landing gear geometry is constrained by wing position, engine clearance, takeoff rotation, and tip-over criteria. In addition to being able to withstand nominal static and dynamic loads, the landing gear also needs to be able to absorb touchdown shock loads. These loads and the required geometry determine the weight of the gear. Many of the constraints imposed on landing gear design are described in [27] and [31].

A. Model Assumptions

The landing gear model assumes a conventional and retractable tricycle landing gear configuration for narrowbody commercial aircraft such as a Boeing 737-800. The nose gear consists of a single strut supported by two wheels. The main gear consists of two struts mounted in the inboard section of the wings, each supported by two wheels. The model only takes one CG location as an input, i.e. it does not consider CG travel. It is also assumed that the main landing gear retracts towards the centerline of the aircraft, rotating about the x axis.

B. Model Description

The landing gear model has 46 free variables and 54 constraints.

Table 11: Free variables in the landing gear model

Free Variables	Units	Description
B	[m]	Landing gear base
E_{land}	[J]	Max KE to be absorbed in landing
F_{w_m}	[-]	Weight factor (main)
F_{w_n}	[-]	Weight factor (nose)
I_m	[m ⁴]	Area moment of inertia (main strut)
I_n	[m ⁴]	Area moment of inertia (nose strut)
L_m	[N]	Max static load through main gear
L_n	[N]	Min static load through nose gear
$L_{n_{dyn}}$	[N]	Dyn. braking load, nose gear
L_{w_m}	[N]	Static load per wheel (main)
L_{w_n}	[N]	Static load per wheel (nose)
S_{sa}	[m]	Stroke of the shock absorber
T	[m]	Main landing gear track
W	[lbf]	Total aircraft weight
W_{lg}	[lbf]	Weight of landing gear

W_{mg}	[lbf]	Weight of main gear
W_{ms}	[lbf]	Weight of main struts
W_{mw}	[lbf]	Weight of main wheels (per strut)
W_{ng}	[lbf]	Weight of nose gear
W_{ns}	[lbf]	Weight of nose strut
W_{nw}	[lbf]	Weight of nose wheels (total)
$W_{wa,m}$	[lbf]	Wheel assembly weight for single main gear wheel
$W_{wa,n}$	[lbf]	Wheel assembly weight for single nose gear wheel
Δx_m	[m]	Distance b/w main gear and CG
Δx_n	[m]	Distance b/w nose gear and CG
$\tan(\phi)$	[–]	Angle b/w main gear and CG
$\tan(\psi)$	[–]	Tip over angle
$d_{nacelle}$	[m]	Nacelle diameter
d_{oleo}	[m]	Diameter of oleo shock absorber
d_{tm}	[in]	Diameter of main gear tires
d_{tn}	[in]	Diameter of nose gear tires
l_m	[m]	Length of main gear
l_n	[m]	Length of nose gear
l_{oleo}	[m]	Length of oleo shock absorber
r_m	[m]	Radius of main gear struts
r_n	[m]	Radius of nose gear struts
t_m	[m]	Thickness of main gear strut wall
t_n	[m]	Thickness of nose gear strut wall
w'_{tm}	[m]	Width of main tires
w'_{tn}	[m]	Width of nose tires
x_m	[m]	x-location of main gear
x_n	[m]	x-location of nose gear
x_{CG}	[m]	x-location of CG
y_m	[m]	y-location of main gear (symmetric)

Table 12: Fixed variables in the landing gear model

Constants	Units	Description
E	[GPa]	Modulus of elasticity, 4340 steel
K	[–]	Column effective length factor
N_s	[–]	Factor of safety
η_s	[–]	Shock absorber efficiency
λ_{LG}	[–]	Ratio of max to static load
ρ_{st}	$[\frac{kg}{m^3}]$	Density of 4340 Steel
σ_{yc}	[Pa]	Compressive yield strength 4340 steel
$\tan(\gamma)$	[–]	Dihedral angle
$\tan(\phi_{min})$	[–]	Lower bound on phi
$\tan(\psi_{max})$	[–]	Upper bound on psi
$\tan(\theta_{max})$	[–]	Max rotation angle
d_{fan}	[m]	Fan diameter
$f_{add,m}$	[–]	Proportional added weight, main
$f_{add,n}$	[–]	Proportional added weight, nose
g	$[\frac{m}{s^2}]$	Gravitational acceleration
h_{hold}	[m]	Hold height
$h_{nacelle}$	[m]	Min. nacelle clearance
n_{mg}	[–]	Number of main gear struts
n_{wps}	[–]	Number of wheels per strut

p_{oleo}	$[\frac{\text{lb}_f}{\text{in}^2}]$	Oleo pressure
$t_{nacelle}$	$[\text{m}]$	Nacelle thickness
w_{ult}	$[\frac{\text{ft}}{\text{s}}]$	Ultimate velocity of descent
y_{eng}	$[\text{m}]$	Spanwise loc. of engines
z_{CG}	$[\text{m}]$	CG height relative to bottom of fuselage
z_{wing}	$[\text{m}]$	Height of wing relative to base of fuselage

1. Landing Gear Position

The landing gear track and base are defined relative to the x- and y-coordinates of the nose and main gear.

$$T = 2y_m \quad (215)$$

$$x_m \geq x_n + B \quad (216)$$

The geometric relationships between the x-coordinates of the main gear, nose gear and the CG position must be enforced. These relationships are:

$$x_n + \Delta x_n = x_{CG} \quad (217)$$

$$x_{CG} + \Delta x_m = x_m \quad (218)$$

Equations (217) and (218) must be satisfied exactly, meaning the constraints that enforce them must be tight. As will be shown below, the load through the nose gear and main gear is proportional to the distance from the CG to the main and nose gear respectively. Because there is downward pressure on these loads - more load generally means heavier landing gear - there is also downward pressure on the distances Δx_n and Δx_m . Therefore signomial constraints are used for both relationships.

$$x_n + \Delta x_n \geq x_{CG} \quad (219)$$

$$x_{CG} + \Delta x_m \geq x_m \quad (220)$$

The main gear position in the spanwise (y) direction is, on one side, lower bounded by the length of the gear itself and, on the other side, upper bounded by the spanwise location of the engines. Both of these constraints are necessary to allow the landing gear to retract in the conventional manner for typical narrowbody commercial aircraft.

$$y_m \geq l_m \quad (221)$$

$$y_m \leq y_{eng} \quad (222)$$

2. Wing Vertical Position and Engine Clearance

The difference between the lengths of the main gear and nose gear is constrained by the vertical position of the wing with respect to the bottom of the fuselage, as well as the spanwise location of the main gear and the wing dihedral. This relationship is a signomial constraint.

$$l_n + z_{wing} + y_m \tan(\gamma) \geq l_m \quad (223)$$

For aircraft with engines mounted under the wing, the length of the main gear is also constrained by the engine diameter, because the engines must have sufficient clearance from the ground. A

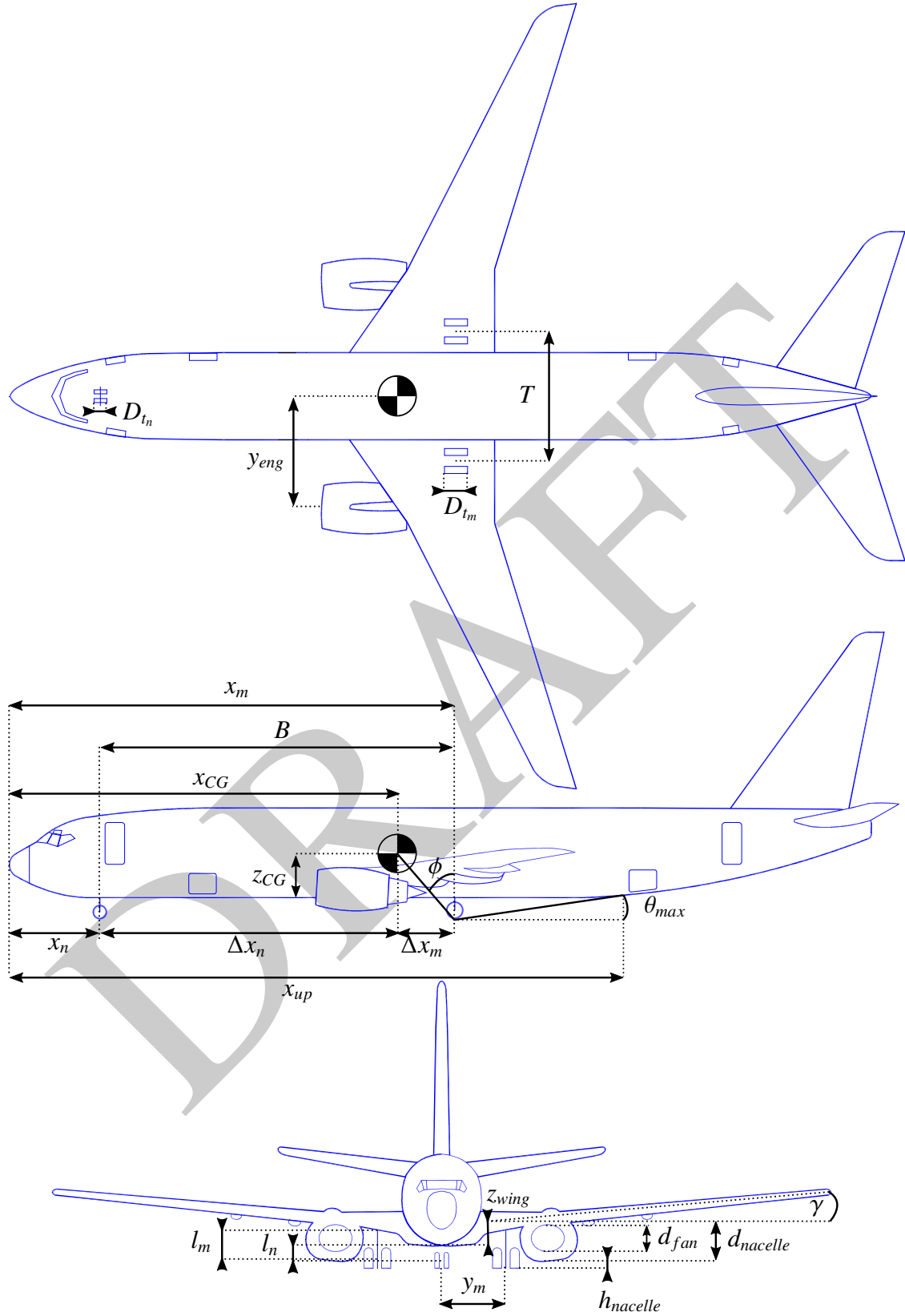


Figure 9: Geometric variables of the landing gear model (adapted from [21])

signomial constraint provides another lower bound on the length of the main gear.

$$l_m + (y_{eng} - y_m) \tan(\gamma) \geq d_{nacelle} + h_{nacelle} \quad (224)$$

$$d_{nacelle} \geq d_{fan} + 2t_{nacelle} \quad (225)$$

3. Takeoff Rotation

The aircraft must be able to rotate on its main wheels at takeoff without striking the tail of the fuselage and, similarly, must be able to land on its main gear without striking the tail [27]. This constrains the location of the main gear. More specifically, the horizontal distance between the main gear and the point at which the fuselage sweeps up towards the tail must be sufficiently small, relative to the length of the main gear, such that the angle relative to the horizontal from the main wheels to the upsweep point is greater than the takeoff/landing angles. The result is a signomial constraint that imposes a lower bound on the length of the gear and the x-location of the main gear.

$$\frac{l_m}{\tan(\theta_{max})} \geq x_{up} - x_m \quad (226)$$

4. Tip-over Criteria

A longitudinal tip-over criterion requires that the line between the main gear and the CG be at least 15° relative to the vertical such that the aircraft will not tip back on its tail at a maximum nose-up attitude [27]. This puts a lower bound on the x-location of the main gear, as measured from the nose of the aircraft. Note that $\tan(\phi)$ is a design variable here, instead of ϕ , to make the constraint SP-compatible.

$$x_m \geq (l_m + z_{CG}) \tan(\phi) + x_{CG} \quad (227)$$

$$\tan(\phi) \geq \tan(\phi_{min}) \quad (228)$$

A lateral tip-over constraint is introduced to ensure that an aircraft does not tip over in a turn [31]. The turnover angle is defined as

$$\tan \psi = \frac{z_{CG} + l_m}{\Delta x_n \sin \delta} \quad (229)$$

where

$$\tan \delta = \frac{y_m}{B}. \quad (230)$$

Using the relationship

$$\cos\left(\arctan\left(\frac{y_m}{B}\right)\right) = \frac{B}{\sqrt{B^2 + y_m^2}}, \quad (231)$$

this constraint can be rewritten in, not only SP-compatible, but GP-compatible form as

$$1 \geq \frac{(z_{CG} + l_m)^2 (y_m^2 + B^2)}{(\Delta x_n y_m \tan(\psi))^2}. \quad (232)$$

Typically this angle, ψ , should be no larger than 63° [27].

$$\tan(\psi) \leq \tan(\psi_{max}) \quad (233)$$

5. Landing Gear Weight

The total landing gear system weight is lower bounded by accounting for the weights of each assembly. An additional weight fraction is used to account for weight that is proportional to the weight of the wheels [32].

$$W_{lg} \geq W_{mg} + W_{ng} \quad (234)$$

$$W_{mg} \geq n_{mg} (W_{ms} + W_{mw}(1 + f_{add_m})) \quad (235)$$

$$W_{ng} \geq W_{ns} + W_{nw}(1 + f_{add_n}) \quad (236)$$

The weight of each strut for both the main and nose struts is lower bounded by simplistically assuming a thin-walled cylinder with constant cross sectional area.

$$W_{ms} \geq 2\pi r_m t_m l_m \rho_{st} g \quad (237)$$

$$W_{ns} \geq 2\pi r_n t_n l_n \rho_{st} g \quad (238)$$

It is assumed that the strut is sized by compressive yield and, more stringently, by buckling, again assuming a thin-walled cylinder. This constrains the area moment of inertia of the strut cross section, which puts upward pressure on the radius and thickness of the struts. The buckling constraint assumes that no side force is exerted on the cylinder, which is perhaps a weak assumption due to forces exerted in braking, for example, and due to the fact that aircraft do not typically land with the main gear struts perfectly normal to the runway surface.

$$2\pi r_m t_m \sigma_{yc} \geq \frac{\lambda_{LG} L_m N_s}{n_{mg}} \quad (239)$$

$$2\pi r_n t_n \sigma_{yc} \geq (L_n + L_{n_{dyn}}) N_s \quad (240)$$

$$L_m \leq \frac{\pi^2 E I_m}{K^2 l_m^2} \quad (241)$$

$$I_m = \pi r_m^3 t_m \quad (242)$$

$$L_n \leq \frac{\pi^2 E I_n}{K^2 l_n^2} \quad (243)$$

$$I_n = \pi r_n^3 t_n \quad (244)$$

A machining constraint is used to ensure that the strut walls are not too thin to be fabricated [31].

$$\frac{2r_m}{t_m} \leq 40 \quad (245)$$

$$\frac{2r_n}{t_n} \leq 40 \quad (246)$$

The wheel weights can be estimated using historical relations from [27, 32], which are, again, conveniently in monomial form.

$$W_{mw} = n_{wps} W_{wa,m} \quad (247)$$

$$W_{nw} = n_{wps} W_{wa,n} \quad (248)$$

$$W_{wa,m} = 1.2 F_{w_m}^{0.609} \quad (249)$$

$$F_{wm} = L_{wm} d_{tm} \quad (250)$$

$$L_{wm} = \frac{L_m}{n_{mg} n_{wps}} \quad (251)$$

$$W_{wa,n} = 1.2 F_{wn}^{0.609} \quad (252)$$

$$F_{wn} = L_{wn} d_{tn} \quad (253)$$

$$L_{wn} = \frac{L_n}{n_{wps}} \quad (254)$$

$$d_{tm} = 1.63 L_{wm}^{0.315} \quad (255)$$

$$w_{tm} = 0.104 L_{wm}^{0.480} \quad (256)$$

$$d_{tn} = 0.8 d_{tm} \quad (257)$$

$$w_{tn} = 0.8 w_{tm} \quad (258)$$

Main gear tyre size can also be estimated using statistical relations. The nose gear tyres are assumed to be 80% of the size of the main gear tyres.

$$d_{tm} = 1.63 L_{wm}^{0.315} \quad (259)$$

$$w_{tm} = 0.104 L_{wm}^{0.480} \quad (260)$$

$$d_{tn} = 0.8 d_{tm} \quad (261)$$

$$w_{tn} = 0.8 w_{tm} \quad (262)$$

In addition, simple retraction space constraints are used to ensure that the gear assemblies are not too wide to fit inside the fuselage.

$$2w_{tm} + 2r_m \leq h_{hold} \quad (263)$$

$$2w_{tn} + 2r_n \leq 0.8 \text{ [m]} \quad (264)$$

6. Landing Gear Loads

The maximum static load through the nose and main gear is constrained by the weight of the aircraft and the relative distances from the CG to the main and nose gear, respectively.

$$L_n = \frac{W \Delta x_m}{B} \quad (265)$$

$$L_m = \frac{W \Delta x_n}{B} \quad (266)$$

For the nose gear, there is an additional dynamic load due to the braking condition. A typical braking deceleration of 3m/s^2 is assumed [27].

$$L_{n,dyn} \geq 0.31 W \frac{l_m + z_{CG}}{B} \quad (267)$$

The nose gear requires adequate load for satisfactory steering performance. A typical desirable range is between 5% and 20% of the total load [27].

$$\frac{L_n}{W} \geq 0.05 \quad (268)$$

$$\frac{L_n}{W} \leq 0.2 \quad (269)$$

7. Shock Absorption

Oleo-pneumatic shock absorbers are common to landing gear for large aircraft. Their purpose is to reduce the vertical load on the aircraft at touchdown, and they are typically sized by a hard landing condition. The maximum stroke of the shock absorber can be determined by considering the aircraft's kinetic energy, and the target maximum load [33].

$$E_{land} = \frac{W}{2g} w_{ult}^2 \quad (270)$$

$$S_{sa} = \frac{1}{\eta_s} \frac{E_{land}}{L_m \lambda_{LG}} \quad (271)$$

As a preliminary model, the oleo size can be estimated using historical relations that are conveniently in monomial form [27]. The length of the main gear must be greater than the length of the oleo and the radius of the tyres.

$$l_{oleo} = 2.5 S_{sa} \quad (272)$$

$$d_{oleo} = 1.3 \sqrt{\frac{4 \lambda_{LG} L_m / n_{mg}}{p_{oleo} \pi}} \quad (273)$$

$$l_m \geq l_{oleo} + \frac{d_{t_m}}{2} \quad (274)$$

VIII. Model Solution

Combining all of the previously described system and subsystem models into one large full-aircraft optimization problem allows us to capture the coupled nature of aircraft design. From a practical perspective, the procedure of combining the subsystem models is relatively straightforward, because, as mentioned previously, each model is fundamentally just a list of constraints. Coupling models essentially just involves concatenating these lists.

When fully combined, the aircraft model has 294 constraints. The free variables that are common to two or more of the subsystem models are illustrated in Figure 10.

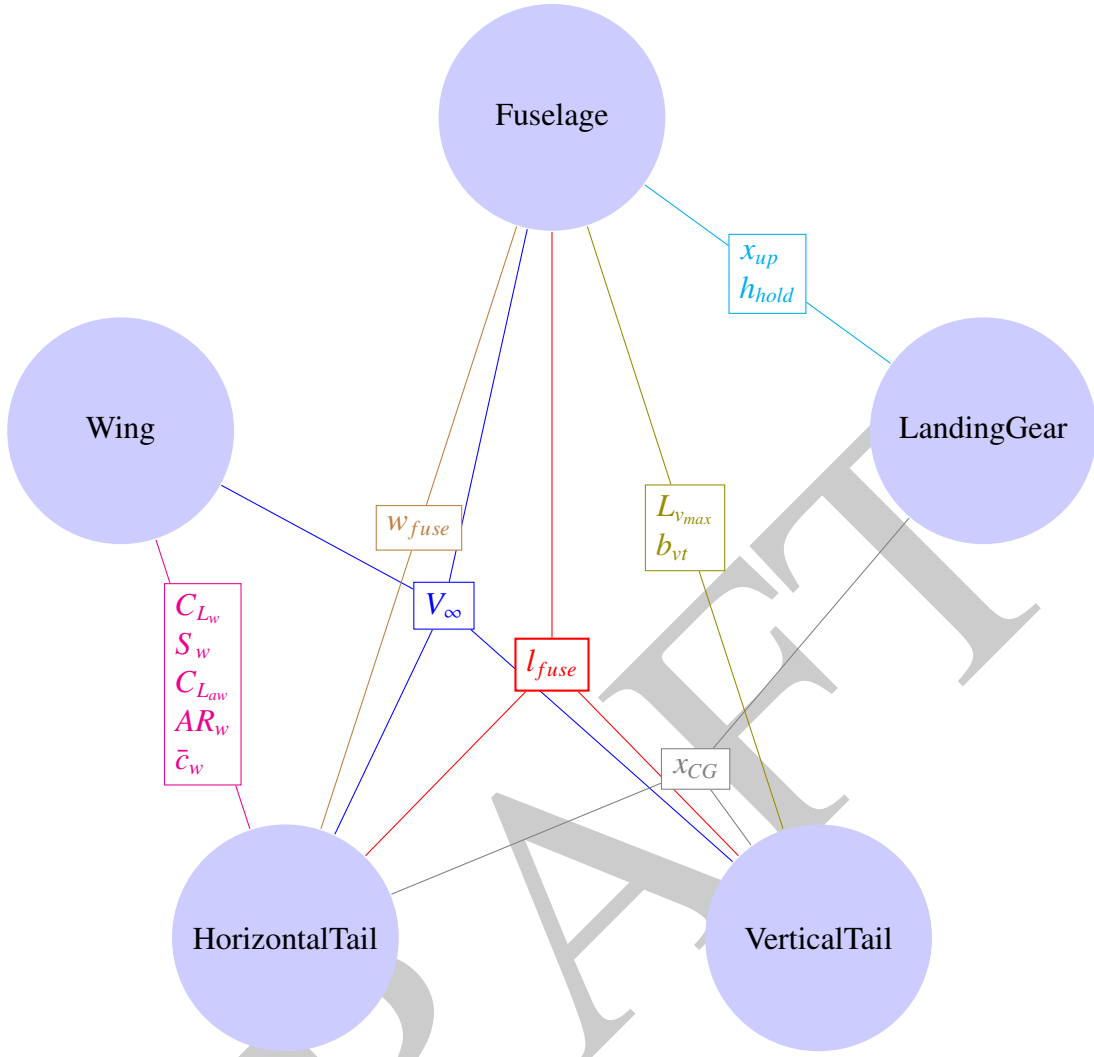


Figure 10: An illustration of how free variables link each of the subsystem models

A. Solution time

The size of the full-system model and therefore its solution time depends on the number of discretizations of the Breguet range model. With two cruise segments the SP has 824 free variables and takes seven GP solves to converge in a time of 6.2 seconds, using a standard laptop computer with a 2.5 GHz Intel Core i7 processor.

B. Convergence of the objective function

Convergence of the objective function (19) is plotted in Figure 11a. The total cost can be decomposed into a contribution from slack variables and a contribution from fuel burn. These decompositions are plotted in Figure 11c. The fuel burn cost contribution for GP iterations three through seven is plotted in Figure 11b, where it is equivalent to the total cost since all slack variables are equal to one after the second GP iteration.

C. Solution comparison to the reference aircraft

The optimal values for a selection of key design variables are presented in Table 13. Discrepancies between computed values and reference aircraft values are largely due to the placeholder engine model and lack of a detailed flight profile, and specifically the lack of a climb flight condition, which particularly affects the sizing of the horizontal tail. Both a detailed engine and flight profile model are the subject of ongoing work. Additionally, total fuel burn is minimized in the presented work, whereas an aircraft manufacturer likely optimizes a more nuanced objective function, including manufacturing cost, maintainability, and the ability to stretch the aircraft in the future. This likely contributes to the discrepancy between the presented values. The ability of the SP aircraft model to robustly solve for alternate objective functions is discussed in future work.

D. Sensitivity to initial guess

As mentioned in the introduction, signomial programs require an initial guess for the subset of variables that appear either on the greater side of signomial inequality constraints or in signomial equality constraints. The solution was obtained using an initial guess of one for each of these variables. To see how sensitive this solution is to the choice of initial guess, the problem was also solved using an order-of-magnitude initial guess for each variable. Using the better initial guess did not change the solution values, and only slightly reduced the solution time (less than 0.1s), largely because any speed increases are mostly limited to the first GP solve, which constitutes a small portion of total solve time.

E. Sensitivity to fixed parameters

The sensitivity of the objective function to each parameter is obtained from the problem's dual solution, at no additional computational cost. Intuitively, the sensitivity is an estimate of the percentage change in the objective value with a one percent change in the value of the parameter. Select sensitivities are presented in Table 14 and discussed below.

At the optimal solution, the objective function is, perhaps unsurprisingly, sensitive to minimum cruise Mach number M_{min} (0.530) and the range requirement R_{req} (1.23). The sensitivity to $W_{avg,pass_{total}}$ is 0.544, which shows that uncertainties in assumptions made about payload can have strong effects on aircraft sizing.

Parameters that are primarily devoted to ensuring safety, such as never-exceed speed V_{ne} and engine y-location y_{eng} , have relatively high sensitivities of 0.425 and 0.510 respectively, giving an example of the safety-performance tradeoff.

The sensitivity to wing maximum lift coefficient, $C_{L_{w,max}}$, is negative (-0.236), but weakly so due to opposing pressures from takeoff sizing and structural sizing constraints. A higher maximum lift can mean lower wing area for a takeoff sizing case (demonstrated by the strong negative sensitivity on V_1 of -0.959), but wing structural constraints mitigate the negative sensitivity, since a higher maximum lift coefficient results in greater wing root moments at a given load factor. The same opposing pressures mean that the sensitivity to horizontal tail maximum lift coefficient $C_{L_{ht,max}}$ is weakly positive (0.0336), showing that structural considerations dominate the aerodynamic forces in the effect of $C_{L_{ht,max}}$ on fuel burn. The model demonstrates that the sensitivities to parameters involved in similar sets on constraints, such as $C_{L_{w,max}}$ and $C_{L_{ht,max}}$, have different signs due to functional differences of the wing and the horizontal tail.

F. Solution behavior with variation in fixed parameters

Sensitivities provide local gradient information about the objective function with respect to variation in fixed parameters. However, if a designer would like to understand the effect of larger changes in fixed parameters, solving the optimization problem over a sweep of the parameters of interest is required. With most MDO methods, the computational cost of these sorts of sweeps would be prohibitive, but the speed of SP's largely mitigates this issue. The first function of sweeps is to allow designers to better explore the topography of the objective function. As an example, 20 aircraft with 150 to 210 passengers were optimized, a range of passengers which is reasonable for an aircraft with 6 seats per row. The results for the fuel weight objective function, and the dry weight of the aircraft, are shown in Figure 12.

Each solution in the parameter sweeps gives the values of all free variables, and the sensitivities to all fixed parameters. Furthermore, through the addition of dummy variables, the sensitivity to constraints can be determined. For example, for a range of n_{pass} , the sensitivities to different components weights are plotted in Figure 13, giving insight into the tradeoffs inherent to a configuration. The decreasing sensitivity to vertical tail weight, and increasing sensitivity to fuselage weight in Figure 13 indicates the effects of a longer fuselage on the fuselage and vertical tail weight trade. As the number of passengers increases, the growing vertical tail moment arm allows for a reduction of the required vertical tail area, which reduces weight and drag. This fuel burn benefit is offset by the fuselage weight growth due to a larger fuselage volume and length, driven especially by the growth of bending material weights as the fuselage lengthens.

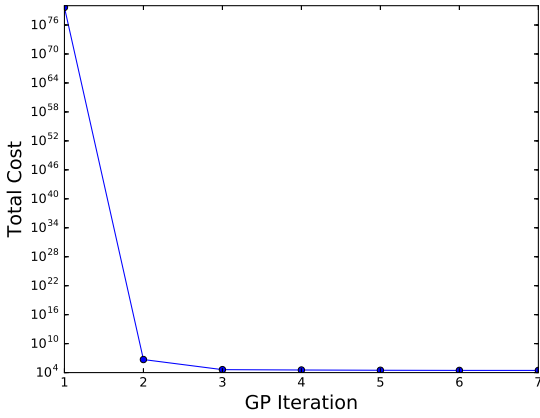
IX. Conclusion

In this work, signomial programming has been used to tackle the multidisciplinary design optimization of a commercial aircraft. More specifically, signomial programming models have been created to find the optimal preliminary sizing of a tube-and-wing-configuration aircraft's wing, vertical tail, horizontal tail, fuselage, and landing gear. These subsystem models have been combined into a single monolithic signomial program that captures the coupled nature of aircraft design.

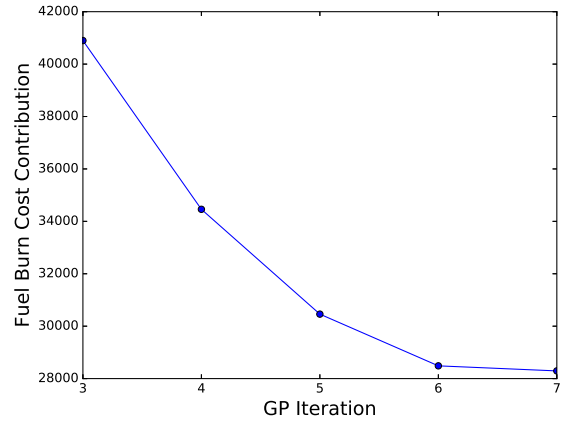
In doing this work, signomial programming has been demonstrated as a viable approach to multidisciplinary aircraft design optimization, with a wide range of constraints fitting naturally into the required formulation. Though not as rigorous as for geometric programs, the solution method for signomial programs is disciplined and effective. A significant improvement in fidelity over previous geometric programming models has been achieved thanks to the relaxed restrictions on signomial programs. Lagrange multipliers obtained from the solution procedure mean that, in addition to finding an optimal design, the models also give local sensitivities to fixed variables, thus giving insight into the design space.

Acknowledgments

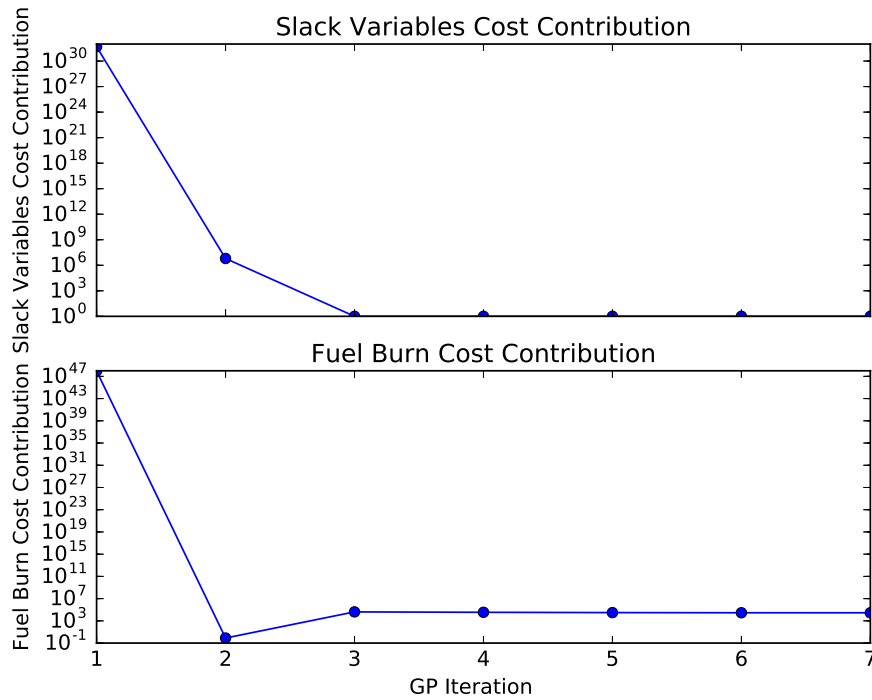
This work was partially funded by the NASA Aeronautics Fellowship as well as Aurora Flight Sciences.



a) Total cost vs GP iteration.



b) Cost contribution of fuel burn for GP iterations with no relaxed constants. Since all slack variables are equal to one, the fuel burn cost contribution is equivalent to total cost.



c) Cost contribution of slack variables and fuel burn vs GP iteration.

Figure 11: Plots illustrating the convergence of the objective function.

Table 13: Key solution variables with comparison to the reference aircraft, where possible. Values marked with * are mean values over the discretized cruise.

Free Variable	Solution Value	Estimate for reference aircraft
Aircraft		
W_{dry} [lbf]	90,789	92822 [23]
D [N]	34,241 *	N/A
$\left(\frac{L}{D}\right)$ [-]	19.7 *	N/A
Wing		
\mathcal{R}_w [-]	10.2	9.5 [23]
b_w [m]	35.8	35.9 [23]
S_w [m ²]	126.0	124.6 [23]
W_w [lbf]	20,533	N/A
D_w [N]	17,344 *	N/A
Vertical Tail		
\mathcal{R}_{vt} [-]	2.00	1.91 [23]
b_{vt} [m]	8.35	7.16 [23]
S_{vt} [m ²]	34.9	26.4 [23]
W_{vt} [lbf]	3,990	N/A
D_{vt} [N]	6,548 *	N/A
Horizontal Tail		
\mathcal{R}_{ht} [-]	6.4	6.2 [23]
b_{ht} [m]	12.3	14.4 [23]
S_{ht} [m ²]	23	32.8 [23]
W_{ht} [lbf]	629	N/A
D_{ht} [N]	1,505 *	N/A
$S.M.$ [-]	0.15 *	N/A
Fuselage		
R_{fuse} [m]	1.85	1.88 [21]
l_{fuse} [m]	36.6	39.1 [21]
W_{fuse} [kg]	16,039	N/A
D_{fu} [N]	8,844 *	N/A
Landing Gear		
B [m]	13.6	15.6 [23]
T [m]	9.8	5.8 [23]
d_{lm} [in]	45	44.5 [23]
W_{lg} [lbf]	3,304	N/A

Table 14: List of selected sensitivities to aircraft parameters

Variable	Sensitivity	Value	Units
System			
M_{min}	0.530	0.800	[-]
R_{req}	1.23	3000	[nmi]
V_{ne}	0.425	144	$[\frac{m}{s}]$
y_{eng}	0.510	4.88	[m]
Wing			
$C_{Lw,max}$	-0.236	2.79	[-]
Vertical Tail			
V_1	-0.959	70.0	$[\frac{m}{s}]$
Horizontal Tail			
$C_{Lht,max}$	0.0336	2.00	[-]
Fuselage			
$W_{avg.pass_{total}}$	0.544	180	[lbf]

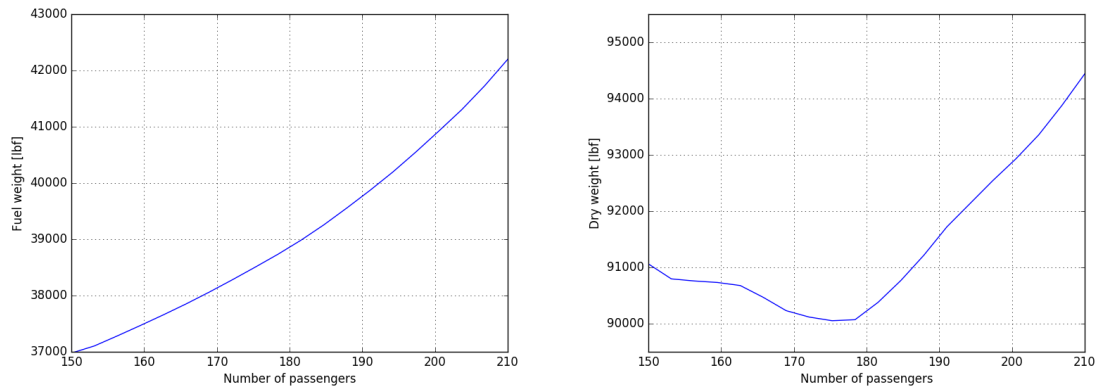


Figure 12: Variation of fuel weight and dry weight with number of passengers

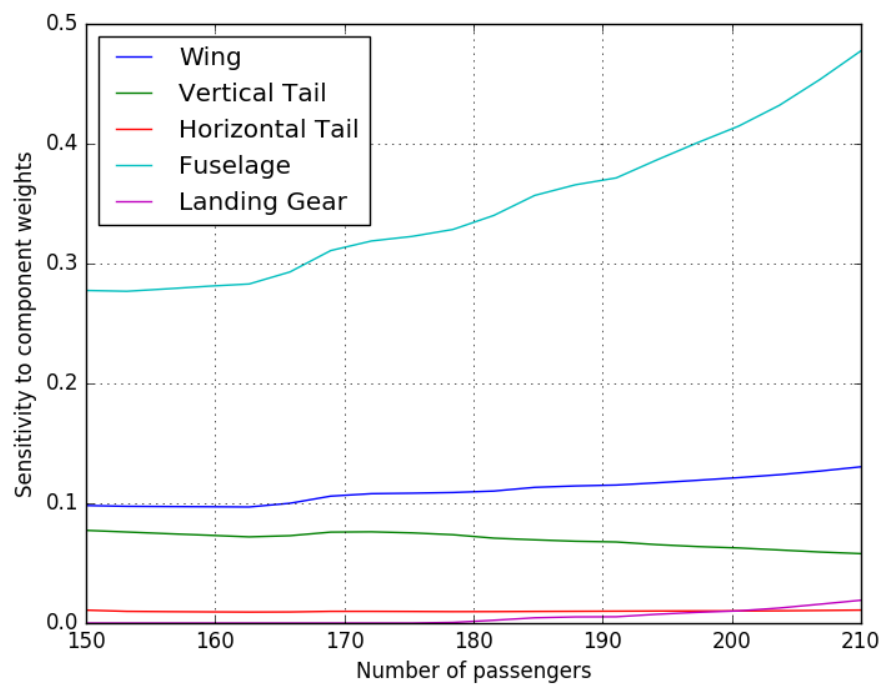


Figure 13: Sensitivities to component weights with number of passengers. The diverging sensitivities to fuselage and vertical tail weights indicate the effects of a lengthening fuselage on the subsystems.

References

- [1] Hoburg, W. and Abbeel, P., “Geometric programming for aircraft design optimization,” *AIAA Journal*, Vol. 52, No. 11, 2014, pp. 2414–2426.
- [2] Boyd, S., Kim, S.-J., Vandenberghe, L., and Hassibi, A., “A tutorial on geometric programming,” *Optimization and engineering*, Vol. 8, No. 1, 2007, pp. 67–127.
- [3] Kroo, I., Altus, S., Braun, R., Gage, P., and Sobieski, I., “Multidisciplinary optimization methods for aircraft preliminary design,” *AIAA paper*, Vol. 4325, 1994, pp. 1994.
- [4] Henderson, R. P., Martins, J., and Perez, R. E., “Aircraft conceptual design for optimal environmental performance,” *Aeronautical Journal*, Vol. 116, No. 1175, 2012, pp. 1.
- [5] Drela, M., *TASOPT 2.08 Transport Aircraft System OPTimization*, 2011.
- [6] de Weck, O., Agte, J., Sobieski, J., Arendsen, P., Morris, A., and Spieck, M., “State-of-the-art and future trends in multidisciplinary design optimization,” *Proceedings of the 48th AIAA/ASME/ASCE/AHS/ASC Structures, Structural Dynamics, and Materials Conference*, AIAA, Vol. 1905, 2007.
- [7] Martins, J. R. and Lambe, A. B., “Multidisciplinary design optimization: a survey of architectures,” *AIAA journal*, Vol. 51, No. 9, 2013, pp. 2049–2075.
- [8] Duffin, R. J., Peterson, E. L., and Zener, C., *Geometric programming: theory and application*, Wiley New York, 1967.
- [9] Mehrotra, S., “On the implementation of a primal-dual interior point method,” *SIAM Journal on optimization*, Vol. 2, No. 4, 1992, pp. 575–601.
- [10] Hoburg, W., Kirschen, P., and Abbeel, P., “Data fitting with geometric-programming-compatible softmax functions,” *Optimization and Engineering*, 2016.
- [11] Hilton, W. F., *High-speed aerodynamics*, Longmans, Green, 1951.
- [12] Lipp, T. and Boyd, S., “Variations and extension of the convex concave procedure,” *Optim Eng*, 2015.
- [13] Boyd, S., “Sequential convex programming,” *Lecture Notes, Stanford University*, 2008.
- [14] Opgenoord, M. M. J., Cohen, B. S., and Hoburg, W. W., “Comparison of Algorithms for Including Equality Constraints in Signomial Programming,” Tech. Rep. TR-17-1, Aerospace Computational Design Laboratory (ACDL), Massachusetts Institute of Technology (MIT), Cambridge, Massachusetts, 2017.
- [15] Burnell, E. and Hoburg, W., “GPkit,” <https://github.com/convexopt/gpkit>, 2016, Version 0.4.0.
- [16] ApS, M., *The MOSEK C optimizer API manual. Version 7.1 (Revision 41).*, 2015.
- [17] Anderson, J. D., *Introduction to flight*, Vol. 199, McGraw-Hill Boston, 2005.
- [18] Martin York, W. H. and Drela, M., “Turbofan Engine Sizing and Tradeoff Analysis via Signomial Programming,” *AIAA Journal of Aircraft*, 2017.
- [19] Kirschen, P. G., *Signomial Programming for Aircraft Design*, Master’s thesis, Massachusetts Institute of Technology, Cambridge, MA, 2016.

- [20] Sutherland, W., “LII. The viscosity of gases and molecular force,” *The London, Edinburgh, and Dublin Philosophical Magazine and Journal of Science*, Vol. 36, No. 223, 1893, pp. 507–531.
- [21] Boeing Commercial Airplanes, “737 Airplane characteristics for airport planning,” *Seattle, Washington, USA*, 2007.
- [22] Kroo, I. and Shevell, R., “Aircraft design: Synthesis and analysis,” *Desktop Aeronautics Inc., Textbook Version 0.99*, 2001.
- [23] Brady, C., “The Boeing 737 Technical Site,” <http://www.b737.org.uk>, 2015 (accessed November 1st 2015).
- [24] Drela, M., “XFOIL: An analysis and design system for low Reynolds number airfoils,” *Low Reynolds number aerodynamics*, Springer, 1989, pp. 1–12.
- [25] Kirschen, P. and Hoberg, W., “GPfit,” <https://github.com/convexopt/gpfit>, 2015, Version 0.1.
- [26] Niță, M. and Scholz, D., *Estimating the oswald factor from basic aircraft geometrical parameters*, Deutsche Gesellschaft für Luft-und Raumfahrt-Lilienthal-Oberth eV, 2012.
- [27] Raymer, D. P., “Aircraft Design: A Conceptual Approach,” 1992.
- [28] Anderson, J. D., “Fundamentals of Aerodynamics, 2001,” .
- [29] Burton, M., *Solar-Electric and Gas Powered, Long-Endurance UAV Sizing via Geometric Programming*, Master’s thesis, Massachusetts Institute of Technology, Cambridge, MA, 2017.
- [30] Anderson, J. D., *Fundamentals of Aerodynamics*, McGraw-Hill, New York, New York, 2011.
- [31] Chai, S. T. and Mason, W. H., *Landing gear integration in aircraft conceptual design*, Master’s thesis, Virginia Polytechnic Institute and State University, 1996.
- [32] Currey, N. S., *Landing Gear Design Handbook*, Lockheed-Georgia Company, 1984.
- [33] Torenbeek, E., *Synthesis of subsonic aircraft design*, 1982.